NATIONAL INSTITUTE OF POLAR RESEARCH

ANTARCTIC GEOLOGICAL MAP SERIES
SHEET 39 SKALLEN (REVISED EDITION)

Explanatory Text of Geological Map

of

Skallen, Antarctica (Revised Edition)

Yasuhito OSANAI, Tsuyoshi TOYOSHIMA, Masaaki OWADA,
Toshiaki TSUNOGAE, Tomokazu HOKADA, Warwick A. CROWE,
Takeshi IKEDA, Tetsuo KAWAKAMI, Yoshinobu KAWANO,
Toshisuke KAWASAKI, Masahiro ISHIKAWA,
Yoichi MOTOYOSHI and Kazuyuki SHIRAISHI

NATIONAL INSTITUTE OF POLAR RESEARCH
TOKYO, MARCH 2004

Antarctic Geological Map Series

Sheet 39

Skallen (Revised Edition)

Explanatory Text of Geological Map of Skallen, Antarctica (Revised Edition)

Yasuhito Osanai [1*], Tsuyoshi Toyoshima [2], Masaaki Owada [3], Toshiaki Tsunogae [4], Tomokazu Hokada [5], Warwick A. Crowe [6], Takeshi Ikeda [7], Tetsuo Kawakami [1], Yoshinobu Kawano [8], Toshisuke Kawasaki [9], Masahiro Ishikawa [10], Yoichi Motoyoshi [5] and Kazuyuki Shiraishi [5]

NATIONAL INSTITUTE OF POLAR RESEARCH, TOKYO, MARCH 2004

---

[1] Department of Earth Sciences, Faculty of Education, Okayama University, 3-1-1, Tsushima-naka, Okayama 700-8530.

* Present address: Department of Evolution of Earth Environments, Graduate School of Social and Cultural Studies, Kyushu University, 4-2-1, Ropponmatsu, Fukuoka 810-8560.

[2] Graduate School of Science and Technology, Niigata University, 2-8050, Ikarashi, Niigata 950-2181.

[3] Department of Earth Sciences, Yamaguchi University, 1677-1, Yoshida, Yamaguchi 753-8512.

[4] Institute of Geoscience, University of Tsukuba, Tsukuba 305-8571.

[5] National Institute of Polar Research, 1-9-10, Kaga, Itabashi-ku, Tokyo 173-8515.

[6] Department of Geology and Geophysics, University of Western Australia, Perth 6907, Australia.

[7] Department of Earth and Planetary Sciences, Graduate School of Science, Kyushu University, 33, Hakozaki, Fukuoka 812-8581.

[8] Faculty of Culture and Education, Saga University, 1, Honjo, Saga 840-8502.

[9] Department of Earth Sciences, Faculty of Science, Ehime University, 2-5, Bunkyo-cho, Matsuyama 790-8577.

[10] Geological Institute, Yokohama National University, 79-7, Tokiwadai, Hodogaya-ku, Yokohama 240-8501.

Contents

1. Introduction

Skallen is located at 69°40'S, 39 °25'E on the west coast of Sôya Coast, Lützow-Holm Bay, East Antarctica. The name "Skallen" comes from a Norwegian term for skull, and this area was named by R. Christensen during his exploratory flight for aerial photography in 1937. A geological survey of Skallen was conducted by T. Tatsumi and T. Kikuchi during the 1st Japanese Antarctic Research Expedition (JARE-1) in 1957, followed by geomorphological and limnological surveys by T. Torii, R. Higano, Y. Yoshida and K. Omoto in 1967-69, and J. Hirabayashi, K. Omoto and K. Moriwaki in 1973-74, and a geological survey by H. Ando, M. Yoshida and T. Ishikawa in 1969-72. A geological map of the Skallen area including Skallevikshalsen and Hjartøy was published in 1976 by Yoshida *et al.* as Antarctic Geological Map Series Sheet 9 "Skallen".

Yoshida *et al.* (1976) classified the basement rocks as paragneiss, metabasite, marble, skarn and allied rocks, quartzite, garnet gneissose granite, charnockite, and minor intrusives. They further divided the basement rocks into the Skallen Brown Gneiss Formation, Skallen Lower Calcareous Formation, Skallen Siliceous Formation, and Skallen Upper Calcareous Formation, from bottom to top. Yoshida *et al.* (1976) and Yoshida (1977) reported many types of folds and fractures in the Skallen region. Yoshida (1977) divided the geologic history of the Skallen region into eight stages (D_1 to D_8). Five stages (D_3 to D_7) of folding and last stage (D_8) of conjugate fracturing were distinguished. The D_3-, D_4-, D_5-, D_6-, and D_7-folds were described as a major subhorizontal recumbent anticline, plunging recumbent anticlines and isoclinal folds, plunging open folds, ESE-trending minor folds, and gentle folds and a NE-trending synform, respectively (Yoshida, 1977). The major geologic structures in the geological map of the Skallen region by Yoshida *et al.* (1976) and Yoshida (1977) are the D_3- and D_4-recumbent anticlines (overturned synforms) and the D_4-isoclinal antiform and synform related to the Skallen thrust. Yoshida *et al.* (1976) and Yoshida (1977) considered that repetition of the stratigraphy occurs due to these major folds and thrust structures.

After Yoshida *et al.* (1976), Skallen was revisited by the following geologists and geomorphologists for field surveys.

K. Shiraishi (JARE-21) in 1980
K. Sasaki (JARE-22) in 1981
Y. Motoyoshi, T. Kawasaki, M. Ishikawa (JARE-33) in 1992
M. Hayashi and T. Sawagaki (JARE-34) in 1993
Y. Kawano, M. Arita and K. Naito (JARE-36) in 1995
Y. Osanai, T. Toyoshima, M. Owada, T. Tsunogae, T. Hokada and W. Crowe (JARE-39) in 1997
H. Miura and S. Yoshinaga (JARE-40) in 1999
T. Kawasaki, Y. Kawano, T. Ikeda and T. Kawakami (JARE-44) in 2003
H. Miura, H. Maemoku and S. Iwasaki (JARE-45) in 2004

This explanatory text incorporates new geological, petrological, geochemical and structural results revealed by these workers.

2. Geomorphology and Quaternary geology

2.1. Landforms and Cenozoic geology

Skallen is the third largest outcrop along the Sôya Coast with 14.4 km^2 exposure. As described in Yoshida *et al.* (1976), Skallen is a relatively flat outcrop with a highest elevation of 186 m a.s.l. Glacial striations and grooves are distinctly preserved on the bedrock surface in two major directions; NW-SE and ENE-WSW, suggesting a change in the direction of glacial movement (Yoshida, 1983).

Recently, Sawagaki and Hirakawa (1997, 2002a, b) proposed a new interpretation that sculptured bedforms in the Lützow-Holm Bay region are due to subglacial water erosion, with a meltwater source attributed to a subglacial lake beneath the Mizuho Plateau.

Raised beaches are found on the east coast, but not on the west coast. Omoto (1977) distinguished 15 levels of raised beaches and step landforms below 32.2 m. However, Yoshida (1983) argued that levels above 15 m, and possibly 10 m, have no clear evidence of marine origin, at least in the southern area.

Igarashi *et al.* (1995) reported ^{14}C values using Tandem Accelerator Mass-Spectrometry (TAMS) for shell fossils from Skallen. The samples from Skallen Ôike (lake) and Magoke Misaki (point) yielded ages of 7810 ± 130, 4720 ± 90, 3790 ± 180, and 3180 ± 90 yr B.P., respectively.

2.2. Basement geology

Skallen is geologically and geomorphologically divided into northern, central and southern areas. The northern and southern areas are characterized by the wide distribution of calc-silicate rocks and gentle folding. The central area is characteristically free from calc-silicate rocks and has extensive brownish hornblende gneiss, with a general metamorphic foliation striking ENE-WSW to ESE-WNW and gentle (18-30°) to steep (42-68°) dips. Each area is bounded by E-W trending steeply north-dipping or near vertical thrusts or shear zones, accompanied by mylonites and later pseudotachylite-cataclasite. These thrusts or shear zones cut across the Skallen peninsula with width of several to hundreds of meters and were eroded to form conspicuous valleys.

Skallen is underlain by various kinds of medium- to high-grade metamorphic rocks and three types of pre- to syn-metamorphic and post-metamorphic intrusive rocks (granite, pegmatite and dolerite). The metamorphic rocks from Skallen can be generally classified into twelve types on the regional map scale, as follows:

a) quartzo-feldspathic garnet-biotite gneiss,
b) quartzo-feldspathic garnet gneiss,
c) garnet-sillimanite-spinel gneiss,
d) garnet-orthopyroxene granulite,
e) quartzo-feldspathic garnet-sillimanite gneiss,
f) corundum-spinel-sillimanite-garnet gneiss,
g) garnet-bearing two-pyroxene-hornblende gneiss,
h) garnet-absent two-pyroxene-hornblende gneiss,
i) hornblende gneiss (brown gneiss),

j) calc-silicate rocks and marbles,
k) thin alternation of quartzo-feldspathic, pelitic, calc-silicate and mafic gneisses,
l) granitic biotite gneiss and pegmatitic gneiss.

Metamorphic rocks from Skallen are mainly subdivided into four categories of precursors: (1) pelitic and quartzo-feldspathic rocks (a~e), (2) mafic and intermediate rocks (f~i), (3) calc-silicate rocks (j) and (4) granitic rocks (l).

Thin alternation of quartzo-feldspathic, pelitic, calc-silicate and mafic gneisses (k) form the main constituent of the northern and southern parts of the central area (Plate 1). Relatively thick leucocratic layers of quartzo-feldspathic garnet-biotite gneiss are widespread in the northern and central areas, while melanocratic layers of garnet-absent two-pyroxene-hornblende gneiss are characteristically observed in central and southern areas. Thin layers of garnet-sillimanite-spinel as well as thick melanocratic layers of garnet-bearing two-pyroxene-hornblende gneiss are distributed in the central and southern areas. Brown hornblende gneiss is also found mainly in central and southern

Table 1. Comparison of lithological classification between the present work and Yoshida et al. (1976).

Yoshida *et al.* (1976)		This work
Skallen Upper Calcareous Formation		Not recognized
Skallen Siliceous Formation	Alternations of paragneiss and metabasite	Thin alternation of quartzo-feldspathic, pelitic and mafic gneisses
	Concordant metabasite	Garnet-bearing two-pyroxene-hornblende gneiss and Two-pyroxene-hornblende gneiss
Skallen Lower Calcareous Formation	Alternations of paragneiss and metabasite	Thin alternation of quartzo-feldspathic, pelitic and mafic gneisses
	Alternations of brown gneiss and metabasite	
	Marble	Calc-silicate rock and marble
	Skarn and allied rocks	
Skallen Brown Gneiss Formation	Alternations of brown gneisse, paragneiss and metabasite	Thin alternation of quartzo-feldspathic, pelitic and mafic gneisses
	Metabasites with alternations of brown gneisses	
Intrusive rocks	Garnet gneisose granite	Quartzo-feldspathic garnet-biotite gneiss
	Brown gneissose granodiorite	Hornblende gneiss and Thin alternation of quartzo-feldspathic, pelitic and mafic gneisses
	Discordant metabasite	Two-pyroxene-hornblende gneiss
	Not distinguished	Quartzo-feldspathic garnet gneiss
		Quartzo-fekdspathic garnet-sillimanite gneiss
		Garnet-sillimanite-spinel gneiss
		Corundum-spinel-sillimanite-garnet gneiss
		Garnet-orthopyroxene granulite

areas (Plate 1). Corundum-spinel-sillimanite-garnet gneiss, quartzo-feldspathic garnet gneiss, and garnet-orthopyroxene granulite can be found in the southern area only.

The distribution of each rock type on the geological map is basically identical to Yoshida *et al.* (1976). Fundamental differences of rock classification and interpretation of geological structure of Skallen are summarized as follows:

1) Stratified sequence of "Skallen Brown Gneiss Formation", "Skallen Lower Calcareous Formation" and "Skallen Siliceous Formation", from bottom to top, in Skallen peninsula (Yoshida *et al.*, 1976) is not recognized. Detailed analysis of geological structures in Skallen by the authors does not support any large-scale over-turned structures. Only intrafolial open and gentle synforms and antiforms in northern and southern areas were identified.
2) Widespread rock types of "garnet gneissose granite" and "brown gneissose granodiorite" in the previous work were dealt with as metamorphosed intrusive rocks and distinguished from stratigraphic formations. The latter was classified as intrusive "charnockite" by Yoshida *et al.* (1976). In the present work, both rock types are described as metamorphic rocks.

A comparison of metamorphic rock names in the present and previous studies is given in Table 1.

Pre- to syn-metamorphic intrusive rocks have granitic and pegmatitic affinities with metamorphic and deformation features, and are now described as granitic biotite gneiss and pegmatitic gneiss, respectively. These rocks are found in the northern part of central area. Unmetamorphosed post-metamorphic intrusive granite, pegmatite and dolerite cut metamorphic foliations as thin dikes, which can not be illustrated on the geological map. More detailed descriptions of modes of occurrence, with brief petrographical features of each metamorphic and intrusive rock type are given below.

3. Metamorphic rocks

3.1. Pelitic and quartzo-feldspathic rocks

Pelitic and quartzo-feldspathic rocks are the dominant lithologies in the Skallen area. Various lithologies occur as an alternation of layers, which are generally less than a few meters in thickness. The most common rock types are quartzo-feldspathic garnet gneiss, garnet-biotite gneiss and garnet-sillimanite gneiss. Spinel occurs locally in sillimanite-bearing gneiss. The alternation of pelitic gneiss with mafic or quartzo-feldspathic gneiss occasionally occurs in a relatively wide area, and is denoted as "thin alternation of quartzo-feldspathic and mafic gneiss (Ga)" in geological map. Representative field occurrences of pelitic and quartzo-feldspathic rocks are shown in Plate 2-1.

3.1.1. Quartzo-feldspathic garnet-biotite gneiss (Ggb)

This rock type is one of the main lithologies in the area, and is occasionally interlayered with garnet gneiss, mafic-intermediate orthogneiss, and with garnet-sillimanite gneiss (Plate 2-1b). Observed mineral assemblages are as follows:

1) garnet + biotite + quartz + plagioclase + alkali feldspar,

2) garnet + biotite + quartz + plagioclase,
3) garnet + biotite + quartz + plagioclase + alkali feldspar + spinel.

Zircon, ilmenite and graphite occur in small amounts. Sub-rounded garnet porphyroblasts up to 5 mm in diameter are present. 1 cm megacrysts include fine-grained rounded quartz grains. Sub-idiomorphic biotite grains less than 2 mm long are aligned parallel to the gneissosity (Plate 3-1a). Biotite (up to 2 mm) also occurs as inclusions (<500 μm) in garnet or around garnet grains. Biotite grains sometimes form aggregated clots. Plagioclase and alkali feldspar are normally less than 2 mm in diameter. Quartz is similar in grain size, but occasional elongated grains are up to a centimeter long. Fine-grained spinel is included in garnet in a few cases.

3.1.2. Quartzo-feldspathic garnet gneiss (Gg)

Garnet-bearing and biotite-free quartzo-feldspathic gneiss occurs in map-scale layers across the western part of Skallen Ôike (lake). This lithology occurs more frequently as thinner layers associated with quartzo-feldspathic garnet-biotite gneiss or intercalated with garnet-sillimanite-spinel gneiss (Plate 2-1b, c). This rock type does not show a strong foliation or lineation. The typical mineral assemblage is quartz + plagioclase + garnet + alkali feldspar (Plate 3-1b). Zircon, monazite, graphite and ilmenite are minor phases. Fine-grained magnetite occurs rarely associated with ilmenite. Biotite is normally absent in the matrix and inclusion in garnet. It occasionally occurs locally around garnet or as inclusions in garnet. Garnet occurs as sub-rounded porphyroblasts up to 1 cm in diameter, which have inclusions of quartz, plagioclase, biotite and ilmenite.

3.1.3. Garnet-sillimanite-spinel gneiss (Ggss)

Pelitic gneiss layers including garnet-sillimanite-spinel gneiss are found as three horizons. These pelitic layers are heterogeneously interlayered. Spinel-bearing garnet-sillimanite gneiss occurs as a layer of a few to several tens centimeters thick, and is commonly intercalated with garnet-biotite gneiss and garnet gneiss (Plate 2-1b, e). Observed mineral assemblages of spinel-sillimanite-bearing varieties are as follows:

1) garnet + sillimanite + spinel + quartz + plagioclase + alkali feldspar,
2) garnet + sillimanite + spinel + biotite + quartz + plagioclase + alkali feldspar,
3) garnet + sillimanite + spinel + biotite + quartz + plagioclase.

Garnet commonly occurs as sub-rounded porphyroblastic grains ranging from a few millimeters to a few centimeters across. It commonly includes fine-grained (<50 μm) quartz inclusions, and less commonly sillimanite, spinel and ilmenite inclusions (Plate 3-1c). Sillimanite (200 μm ~ 5 mm) is elongate, and is aligned parallel to gneissosity. Sillimanite occurs locally in the gneiss, and associated with spinel in many cases. Spinel grains are less than 200 μm in diameter, and occur in the matrix and as inclusions in garnet. Spinel occasionally forms aggregates with sillimanite or plagioclase. Other constituents are plagioclase, alkali feldspar, quartz, biotite, zircon, monazite, apatite, rutile, graphite and ilmenite.

Relict minerals such as kyanite and staurolite have been found as inclusions in porphyroblastic garnet in garnet-sillimanite-spinel gneiss (sample 80S14; Plate 3-1f). These relict minerals are interpreted as metastable phases as they never occur in the

matrix where sillimanite is a stable phase. The mode of occurrence suggests that the rocks including these relict minerals have followed a prograde path from the kyanite-staurolite stability field to the garnet-sillimanite-spinel stability field, and this petrographic feature, *i.e.* kyanite inclusions in sillimanite-bearing gneisses, has been found in other localities in Lützow-Holm Complex (*e.g.*, Hiroi *et al.*, 1991).

3.1.4. Garnet-orthopyroxene granulite (Ggo)

This lithology occurs as a map-scale layer at the east of Skallen Ôike (lake). Smaller garnet-orthopyroxene granulite layers and lenses also occur, interleaved with quartzo-feldspathic garnet-biotite gneiss or mafic granulite (Plate 2-1d). Major constituents are quartz, plagioclase, garnet, orthopyroxene, biotite and ilmenite (Plate 3-1d). Zircon, monazite and graphite are minor phases. The rocks are coarse-grained with the grain sizes of garnet, orthopyroxene and quartz up to a centimeter across. Biotite and plagioclase are commonly less than 1 mm across. Plagioclase occasionally occurs around garnet or along garnet-orthopyroxene grain boundaries or garnet-biotite grain boundaries. Biotite occurs both in the matrix and as inclusions in garnet.

3.1.5. Quartzo-feldspathic garnet-sillimanite gneiss (Ggs)

This lithology is characterized by a conspicuous whitish-pink-color (Plate 2-1f). This layer occurs as a map-scale layer in the coastal area east of Skallen Ôike (lake). The typical mineral assemblage is garnet + sillimanite + spinel + quartz + plagioclase + alkali feldspar. The rocks typically lack biotite except as locally patches. Rutile, biotite, zircon, monazite, graphite and ilmenite are minor phases. Garnet is porphyroblastic, with grains up to a centimeter across. Sillimanite is elongate and up to 2 mm long. It normally occurs in the matrix, and as rare inclusions in garnet rims. Spinel, not abundant, is commonly associated with sillimanite.

3.1.6. Corundum-spinel-sillimanite-garnet gneiss (Gcgs)

This lithology only occurs in one horizon in the coastal area east of Skallen Ôike (lake). This gneiss layer is intercalated with quartzo-feldspathic garnet-sillimanite gneiss. Corundum is conspicuously present accompanied by spinel, sillimanite, garnet and plagioclase (Plate 3-1e). Biotite, quartz and Fe-Ti oxides are minor phases. Corundum grains are hypidiomorphic to xenomorphic, and partly rounded with grain sizes up to 500 μm across. It is commonly surrounded by plagioclase. Quartz is not found near corundum grains. Xenomorphic spinel, less than 500 μm in diameter, is also commonly surrounded by plagioclase. Sillimanite is subrounded and elongate up to 1 mm in length. Garnet occurs as porphyroblasts up to 5 mm in diameter.

3.2. Mafic and intermediate rocks

Mafic and intermediate rocks are present as thin intercalations (ranging from several centimeters to meters wide) with layers of quartzo-feldspathic and garnet-biotite gneiss, or as thick layers throughout the area. These occur mostly parallel to the gneissosity in adjacent layers (Plate 2-2a). Occasionally, the gneisses occur as intrusive rock cutting the compositional layering (Plate 2-2d). Although textures and mineral assemblages of the rocks vary among samples, they can be subdivided into

three major rock types: garnet-bearing two-pyroxene-hornblende gneiss, two-pyroxene-hornblende gneiss (garnet-absent), and hornblende gneiss (brown gneiss). Pyroxene-bearing granulite generally occurs as layers of up to 50 m thick, while some thicker (up to 100 m) layers are also present in the southern part of the area. Hornblende gneiss occasionally forms large bodies (up to 200 m across) north of Skallen Ôike (lake). Detailed petrographical and mineralogical descriptions are given below.

3.2.1. Garnet-bearing two-pyroxene-hornblende gneiss

This rock type is characterized by medium- to coarse-grained garnet, orthopyroxene, plagioclase, hornblende and biotite. Accessory minerals include clinopyroxene, quartz, zircon, apatite and ilmenite. Observed mineral assemblages are as follows:

1) garnet + orthopyroxene + plagioclase + hornblende + biotite + quartz,
2) garnet + orthopyroxene + plagioclase + hornblende,
3) garnet + orthopyroxene + plagioclase + biotite + quartz.

Garnet (up to 3 mm, occasionally ~2 cm in diameter) is poikiloblastic and contains inclusions of quartz, plagioclase and biotite. Irregular-shaped garnet grains in some samples show spectacular textures with the development of a corona of symplectitic orthopyroxene + plagioclase (Plates 2-2b, c, 3-2a), suggesting the progress of the following reaction:

$$\text{garnet} + \text{quartz} \rightarrow \text{orthopyroxene} + \text{plagioclase}. \quad (1)$$

This reaction is one of the most common decompressional textures described in intermediate to mafic granulites from many high-grade terranes. Fine-grained (< 0.3 mm) symplectitic aggregates of orthopyroxene and plagioclase in some samples probably suggest a complete consumption of the reactant garnet. Aggregates of biotite around anhedral orthopyroxene suggest hydration of orthopyroxene at a retrograde stage. The following is a possible reaction to explain the texture:

$$\text{orthopyroxene} + \text{K-feldspar} + H_2O \rightarrow \text{biotite} + \text{quartz}. \quad (2)$$

Coarse-grained patches and layers, composed of plagioclase and orthopyroxene, occur in mafic gneisses throughout the area (Plate 2-2e). The coarse-grained and sub- to euhedral crystal shape of the orthopyroxene implies formation by partial melting of host mafic rocks.

Mineral chemistry of a representative granulite sample (sample B97122302F) is briefly discussed below. Analytical results are summarized in ACF diagrams (Fig. 1). Garnet is almandine-rich; rims (Alm_{55-26} Pyr_{24-25} Grs_{14-15} Sps_{4-5}) are slightly more Fe-rich and Mg-poor than the cores (Alm_{54-55} Pyr_{28-29} Grs_{14-15} Sps_{3-4}), probably due to retrograde reequilibration. Compositions of plagioclase vary depending on texture. Generally, matrix medium-grained plagioclase has a lower anorthite content (An_{48-53}) than that in symplectites (An_{76-78}). Orthopyroxene also shows slight compositional variations. X_{Mg} (= Mg/(Fe+Mg)) of matrix coarse-grained orthopyroxene is 0.56-0.57, while that of symplectitic orthopyroxene is 0.55-0.56. Al_2O_3 contents of the two

orthopyroxene varieties are almost identical (0.81-1.21 wt%). Biotite (X_{Mg} = 0.58-0.60) in the sample is characterized by high TiO_2 content (5.2-5.7 wt%). Hornblende is classified as pargasite (X_{Mg} = 0.56-0.57, Si = 6.4-6.5 pfu, Na = 0.44-0.45 pfu, K = 0.30-0.33 pfu) according to the classification of Leake *et al.* (1997).

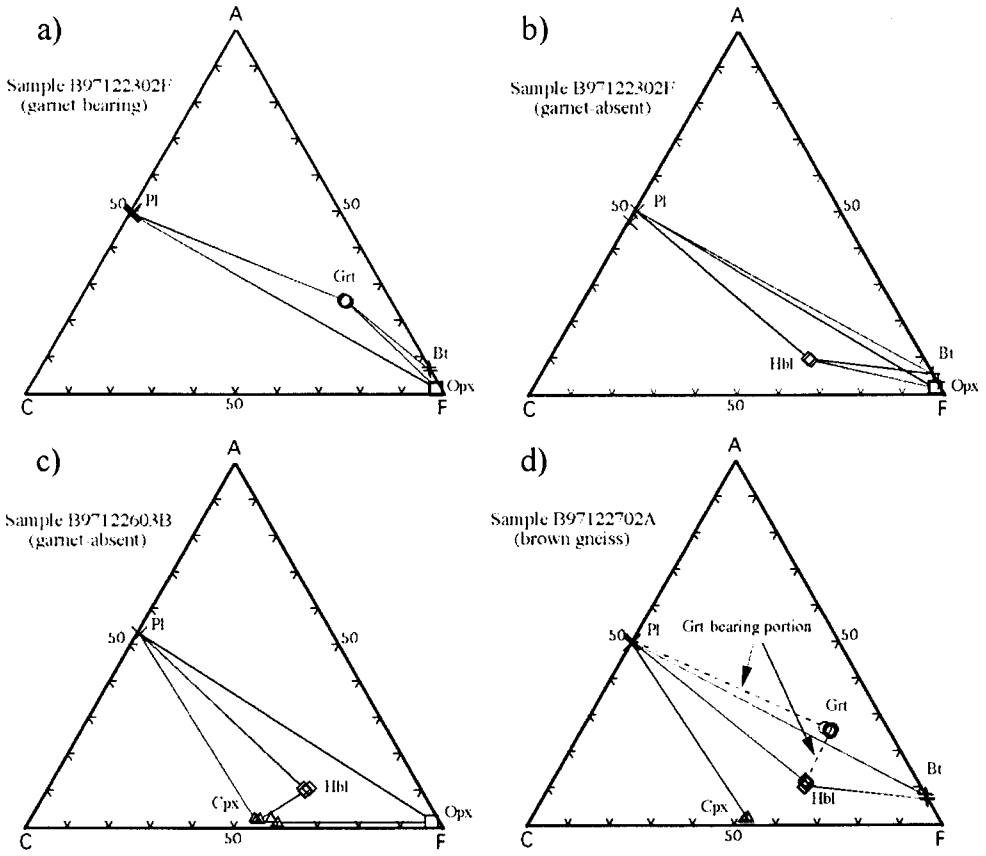

Fig. 1. ACF diagrams showing mineral assemblages and compositions in mafic rocks. (a) Garnet-bearing assemblage in sample B97122302F. (b) Garnet-absent assemblage in sample B97122302F. (c) Two-pyroxene-hornblende assemblage in sample B97122603B. (d) Garnet-bearing variety of brown gneiss (sample B97122702A).

3.2.2. Two-pyroxene-hornblende gneiss (garnet-absent)

This rock type is composed mainly of orthopyroxene, hornblende, plagioclase and clinopyroxene. Accessory minerals are biotite and ilmenite. Lack of garnet is probably due to lower bulk Al_2O_3 content than that of garnet-bearing mafic gneiss. There are some varieties of mineral assemblage as follows:

1) orthopyroxene + hornblende + plagioclase + clinopyroxene + biotite + quartz,
2) orthopyroxene + hornblende + plagioclase + clinopyroxene.

Plate 3-2b shows a typical mineral assemblage of medium- to coarse-grained (0.3-1.5 mm) orthopyroxene, hornblende, plagioclase, clinopyroxene and biotite. It occasionally shows granoblastic texture and no obvious mineral lineations are present. In biotite-free portions of the rock (Plate 3-2c), orthopyroxene is completely surrounded by hornblende, which also suggests retrograde metamorphism. The following reaction is inferred for the texture:

$$\text{orthopyroxene} + \text{plagioclase} + H_2O \rightarrow \text{hornblende} + \text{quartz}. \quad (3)$$

Compositions of minerals in a typical two-pyroxene mafic granulite (B97122603B2) were analyzed by an electron microprobe, as shown in ACF diagrams (Figs. 1b and c). The anorthite content of plagioclase in the sample varies from An_{50} to An_{51}, which is close to that in a garnet-bearing mafic gneiss. X_{Mg} of orthopyroxene and clinopyroxene is 0.42-0.44 and 0.54-0.55, respectively. Hornblende (pargasite) is slightly more rich in K (0.36-0.38 pfu) than in sample B97122302F (garnet-bearing mafic gneiss).

3.2.3. Hornblende gneiss (brown gneiss)

As shown in Fig. 1, this rock type is composed of plagioclase, hornblende and biotite, with or without garnet and clinopyroxene. Zircon and apatite are accessory minerals. This lithology was defined as "brown gneiss" by Yoshida *et al.* (1976) due to its brownish weathered surface (Plate 2-2f). There are some varieties of mineral assemblage as follows:

1) hornblende + plagioclase + biotite + clinopyroxene,
2) hornblende + garnet + plagioclase + clinopyroxene,
3) plagioclase + quartz + hornblende + biotite.

Assemblages 1 and 2 are mafic in composition, while assemblage 3 is dioritic. In hand specimen, the rocks show an obvious foliation defined by quartzo-feldspathic minerals (*e.g.* Plate 2-2f), yet hornblende and biotite are not apparently aligned. Hornblende in assemblage 1 is coarse-grained (0.2-2.5 mm) and dark greenish in color (Plate 3-2d). Biotite (0.3-2.2 mm) is brownish and scattered around hornblende. Clinopyroxene is a rare mineral that occurs mainly in the plagioclase-rich portion of the rock. It is fine-grained (<0.2 mm) and occasionally surrounded by hornblende and biotite. A garnet-hornblende assemblage is present in some samples (Plate 3-2e). Garnet (0.2-0.6 mm) in the sample B97122603A occurs as subhedral aggregates and forms garnet-rich portions in hornblende + plagioclase matrix. It is compositionally almandine-rich (Alm_{54-56} Pyr_{16-18} Grs_{18-20} Sps_{7-9}), which is slightly more Ca-rich than in two-pyroxene-hornblende gneiss. Anorthite content of plagioclase associated with the garnet is also as high as An_{70} to An_{76}. Biotite (X_{Mg} = 0.55-0.56) in the sample is characterized by high TiO_2 content (4.7-4.8 wt%). Hornblende is pargasite (X_{Mg} = 0.50-0.52 and Si = 6.1-6.2 pfu).

3.3. Calc-silicate rocks and marble

Lenticular-shaped blocks or thin intercalations (less than a few tens of meters thick) of pure to impure marble are widespread in the area. These marbles normally coexist with various kinds of skarn-type calc-silicate rocks between marble and surrounding pelitic, quartzo-feldspathic and mafic gneisses (Plate 2-3). Representative photomicrographs of calc-silicate rocks and marbles are shown in Plate 3-3. Calc-silicate rocks have well-layered structures, with compositional layers including the following various mineral assemblages in each area (Plate 2-3).

Constituent minerals of calc-silicate rocks and marbles from the northern most area are relatively simple as follows:

1) spinel + diopside,
2) spinel + phlogopite + forsterite,
3) phlogopite + spinel + dolomite/calcite,

in which euhedral and characteristically coarse-grained purple spinel (up to 7 cm) is observed. Mineral assemblages of calc-silicate rocks and marbles from southern part of the northern area along the boundary shear zone have the following varieties:

4) phlogopite + spinel + forsterite,
5) phlogopite + spinel + diopside + feldspar,
6) scapolite + diopside + phlogopite + feldspar,
7) scapolite + spinel + phlogopite + forsterite + feldspar,
8) scapolite + spinel + phlogopite + diopside + feldspar,
9) grossular + diopside + scapolite + feldspar.

Subordinate amounts of ruby corundum, humite, apatite, titanite, zircon, calcite, dolomite and quartz are also observed, except for impure marble (4) which contains large amounts of calcite and dolomite.

Mineral assemblages of those rocks from the southern area are more complicated:

10) spinel + phlogopite + pargasite + dolomite,
11) olivine + phlogopite + dolomite,
12) spinel + diopside,
13) spinel + diopside + phlogopite + feldspar,
14) spinel + diopside + scapolite + feldspar,
15) scapolite + spinel + phlogopite + diopside + feldspar,
16) scapolite + spinel + phlogopite + pargasite + feldspar.
17) scapolite + spinel + phlogopite + forsterite + feldspar,
18) scapolite + diopside + phlogopite + feldspar,
19) scapolite + diopside + pargasite + feldspar.

Assemblages (10) and (11) are impure marbles and are mostly calcite. Accessory minerals are apatite, corundum, humite, quartz and zircon.

Two samples of zoned scapolite-bearing calc-silicate rock are described here, which are representative of assemblage (6) from the northern area and assemblage (16) from the southern area. The scapolite-diopside-phlogopite rock (assemblage 6: *e.g.* A97122403A) is composed mainly of scapolite, diopside and phlogopite (Plate 3-3) with subordinate amounts of alkali feldspar, apatite, calcite, dolomite and quartz. Scapolite occurs as subhedral to anhedral megacrysts up to 4 cm long, is gray to white in hand specimen and shows remarkable zoning, being poorer in meionite in cores

(Me_{37}) than in rims (Me_{57}) (Kusachi *et al.*, 1999). Pure diopside (X_{Mg} = 0.913-0.944) and small amounts of calcite and dolomite occur as interstitial phases on the boundaries of scapolite grains. Phlogopite (X_{Mg} = 0.905-0.914) occurs as anhedral inclusions in scapolite and diopside. Alkali feldspar (Or_{95-99}) and quartz intergrowths also sporadically occur as a fine veins cutting scapolite.

The scapolite-spinel-phlogopite-pargasite sample (assemblage 16: *e.g.*, A97122705E) contains scapolite, spinel, phlogopite, pargasite, plagioclase, calcite and dolomite (Plate 3-3) with subordinate amounts of apatite, corundum and zircon. Scapolite occurs as subhedral to anhedral grains up to 1.5 cm long, is white in hand specimen and in direct contact with spinel, phlogopite, plagioclase, pargasite, calcite and dolomite. Characteristic zonal structures in scapolite were observed as in sample A97122403A described above, but composition was reversed, with Me_{79} in the core and Me_{35} at the rim. Where it occurs in direct contact with plagioclase (An_{81-86}) and symplectitic intergrowths with plagioclase, scapolite shows a weak zonal structure from Me_{79} in the core to Me_{70} at the rim. Spinel (X_{Mg} = 0.858-0.878) occurs as euhedral to subhedral crystals up to 1 cm across, and is pale blue to greenish blue in hand specimen. Fine-grained spinel inclusions in phlogopite (X_{Mg} = 0.938-0.943), plagioclase and scapolite were also observed. Corundum occurs locally as inclusions in spinel. Pale brown to colorless anhedral pargasite (X_{Mg} = 0.929-0.957) locally occurs between spinel and phlogopite.

3.4. Granitic biotite gneiss

Granitic biotite gneiss is medium-grained and leucocratic, pinkish and brownish in color, and occurs as a layers a few meters to tens of meters thick or as lenses in the central to northwestern part of Skallen. Migmatitic rocks locally occur at the boundary between granitic biotite gneiss and garnet-biotite gneiss (Plate 2-3d), suggesting the protolith of the gneiss was intruded. The gneiss has a weak foliation parallel to the pervasive layering and foliation in neighboring gneisses. Mineral assemblages in granitic biotite gneiss are as follows:

1) biotite + plagioclase + quartz + mesoperthite,
2) garnet + biotite + plagioclase + quartz + alkali feldspar.

In addition to these minerals, the gneiss contains zircon, apatite and Fe-Ti oxides as accessory minerals.

4. Intrusive rocks

In this chapter, we describe igneous lithologies that intruded the basement metamorphic rocks. Emplacement probably took place after the peak metamorphism, but some rocks were deformed during retrograde metamorphism. Intrusive rocks include granite, pegmatite and dolerite.

4.1. Granite

Granite intrudes the host gneisses, and has three modes of occurrence, namely pods, sheets and dikes. In the northeastern part of Skallen, the former two types of granite

are well exposed.

Pod-type granite is leucocratic and medium grained, consisting mainly of plagioclase, quartz and biotite with small amounts of alkali feldspar and garnet. Grain sizes are around 1 to 3 mm across with an equigranular texture. Apatite, zircon and opaque minerals are present as accessory minerals. Quartz is subhedral to anhedral, and usually exhibits weak undulatory extinction. Subhedral plagioclase is partly corroded. Subhedral to anhedral biotite is partly altered to secondary chlorite. Most of this type of granite contains biotite, and refer to pod-type granites as biotite tonalite hereafter.

Granite also occurs as sheets, a few meters thick. This granite is leucocratic and medium-grained, and contains a large amount of alkali feldspar in addition to plagioclase, quartz and biotite, and small amounts of apatite, zircon and opaque mineral. The alkali feldspar is euhedral and perthitic. Subhedral quartz exhibits weak undulatory extinction. Subhedral plagioclase and biotite are partly altered to secondary sericite and chlorite, respectively. The sheet type is hereafter referred to as biotite granite.

A granite dike, 0.3 to 1 meter in width, is exposed in the southern part of Skallen. The dike occurs along a mylonitic shear zone with a N-S strike (Plate 2-3e). Chilled margins, a few centimeters wide, are developed along the intrusive boundary. A foliation is defined by orientation of biotite, parallel to the boundary of the intrusion. The granite dike consists mainly of plagioclase, biotite, alkali feldspar, quartz and muscovite with small amounts of apatite, zircon and opaque mineral (Plate 3-3f). Biotite grains are locally chlolitized. The inner parts of plagioclase grains are generally altered to an aggregation of sericite. This granite is named muscovite-biotite granite and is petrographically distinct from the other two types.

4.2. Pegmatite

Pegmatite is leucocratic or pinkish but locally melanocratic depending on the modal variation of mafic minerals. The pegmatite is locally deformed. Deformed pegmatite dikes are several centimeters to meters wide, and cut foliation and layering in the host gneiss.

Pegmatite dikes occur throughout Skallen. The dikes are up to a few meters in width, and have locally rehydrated the host rocks. The dikes have variable grain sizes and lithologies. Some contain large amounts of tourmaline, and others contain hornblende (Plate 2-3f). Most of the pegmatite dikes intruded along the shear zone in various directions. Mineral assemblages of pegmatite dikes include quartz, alkali feldspar, plagioclase, biotite, hornblende and tourmaline.

4.3. Dolerite

A dolerite dike occurs along a fracture several centimeters wide in the northwestern part of Skallen. The dike vertically intrudes the host gneisses with a sharp contact. Since the intrusive size is small, the dike cannot be shown on the geological map. The dolerite is pale brownish green, moderate- to fine-grained and massive. The mineral assemblage of the dolerite includes clinopyroxene, hornblende and plagioclase.

5. Structural geology

The major geologic structures in Skallen are an E-W trending foliation with E-W trending mineral lineation, ENE-WSW to E-W trending asymmetric intrafolial folds, E-W trending and N-dipping faults, and ENE-WSW to E-W trending open to gentle upright folds. These structures and other minor ones were formed through poly-stage deformation. The E-W trending foliation dips gently to moderately north in the central part of Skallen (Fig. 2b). In the northern and southern parts, poles to the foliations lie on great-circles, corresponding to ENE-WSW to E-W trending open to gentle upright folds (Figs. 2a, c, and d). Attitudes of the great circles are almost the same between the northern and southern parts (Figs. 2a, c, and d).

In the revised geological map, the major geologic structures are an E-W trending and gently to moderately dipping foliation, ENE-WSW to E-W trending asymmetric intrafolial folds, E-W trending and N dipping faults, and ENE-WSW to E-W trending open to gentle upright folds. Yoshida's "recumbent anticlines", "isoclinal folds", and "Skallen thrust" are not shown on the revised map. This is a fundamental difference in the geologic structure from the geological map in Yoshida *et al.* (1976) and Yoshida (1977). The recumbent anticline (overturned synform) near Osiage Hama (beach) has been re-interpreted as geological-map scale intrafolial folds. The recumbent anticline and syncline (overturned synform and antiform) were not recognized near Himi Yama (peak). Moreover, we were not able to confirm the presence of the isoclinal folds (overturned synform and antiform) and their axial foliation in the central to northern part of Skallen. There is no evidence for the duplication of stratigraphy by these folds and "Skallen thrust". The metamorphic rocks in Skallen generally show gently to moderately dipping foliation (Fig. 2). The "Skallen thrust" shown by Yoshida *et al.* (1976) and Yoshida (1977) is a strike-slip fault associated with an E-W trending mineral lineation.

Metamorphic rocks with a well-developed E-W trending foliation and a strong mineral lineation show various kinds of asymmetric structures such as asymmetric intrafolial folds, rotated, shortened, and folded boudins (Plate 2-4a), asymmetric boudinage (Plate 2-2a), and coarse-grained minerals with asymmetrical tails of fine-grained minerals (Plate 2-4b). The asymmetric intrafolial folds are isoclinal to open and have E-W to ENE-WSW trending and gently dipping axial surfaces with horizontal fold axes (Fig. 3a). ENE-WSW to E-W trending asymmetric intrafolial folds on the geological-map scale occur to the northwest of Osiage Hama (beach) (Plate 2-4c). These intrafolial folds are associated with parasitic folds. Most of the asymmetric structures indicate a top-to-the east displacement, namely layer-parallel dextral shearing in the central part. Lens-shaped garnets are found in the well-foliated and lineated metamorphic rocks in some parts of the studied area. The elongate garnets were plastically deformed (Michibayashi *et al.*, 2004). Orthopyroxene + plagioclase coronas (symplectite texture) around garnets grow across the foliation and lineation formed by top-to-the east displacement (Plate 2-2b).

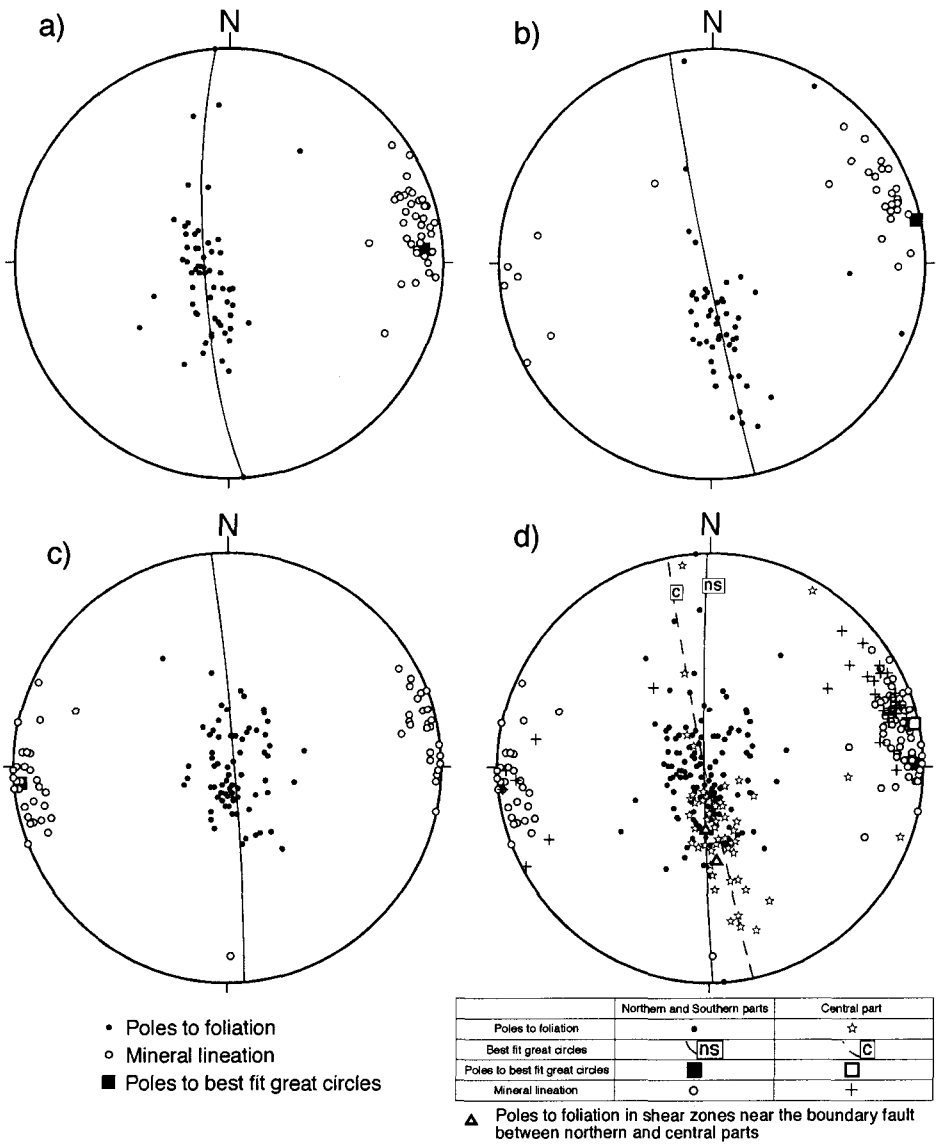

Fig. 2. Lower hemisphere equal area projections of poles to foliation, with best fit great circle, poles to the circles, and mineral lineation. a)northern part, b) central part, c) southern part, d) whole area. Poles to foliation (open triangles) in shear zones near the boundary fault between northern and central parts are shown in d).

Symmetric boudins are found in metamorphic rocks with weak foliation and mineral lineation. The presence of rotated, shortened, and folded boudins and symmetric boudins suggest that layer-normal shortening took place before top-to-the

east displacement.

An asymmetric geological-map scale fold with an S-shaped profile occurs to the northeast of Kado Misaki (point), indicating shearing in a sinistral sense along the E-W trending and N-dipping fault between the northern and central parts. The boundary fault, named the Skallen thrust by Yoshida *et al.* (1976) and Yoshida (1977), is associated with a narrow shear zone where an E-W trending foliation and E-W trending mineral lineation is well developed. From this, the boundary fault (Skallen thrust) is inferred to be a sinistral strike-slip fault. This faulting may be related to locally developed asymmetric structures indicating layer-parallel sinistral shearing.

Most of the ENE-WSW to E-W trending open to gentle upright folds are found in the northern and southern parts. The upright folds (synform and antiform) on the geological-map scale also occur in the northern and southern parts (Plate 2-4c). These upright folds are associated with parasitic folds. The E-W trending foliations are folded by the upright folding (Figs. 2a, c, and d and Plate 2-4d). The intrafolial folds are refolded by the upright folding (Plate 2-4c).

A conjugate-set of NW-SE or N-S trending narrow mylonite zones occur locally in the studied area cutting E-W trending foliations, intrafolial folds, and open to gentle upright folds. The mylonites have vertical to subvertical dipping mylonitic foliations and strong subhorizontal mineral lineations parallel to the zones, and show strike-slip movement. The foliations of the surrounding non-mylonitized gneisses are rotated

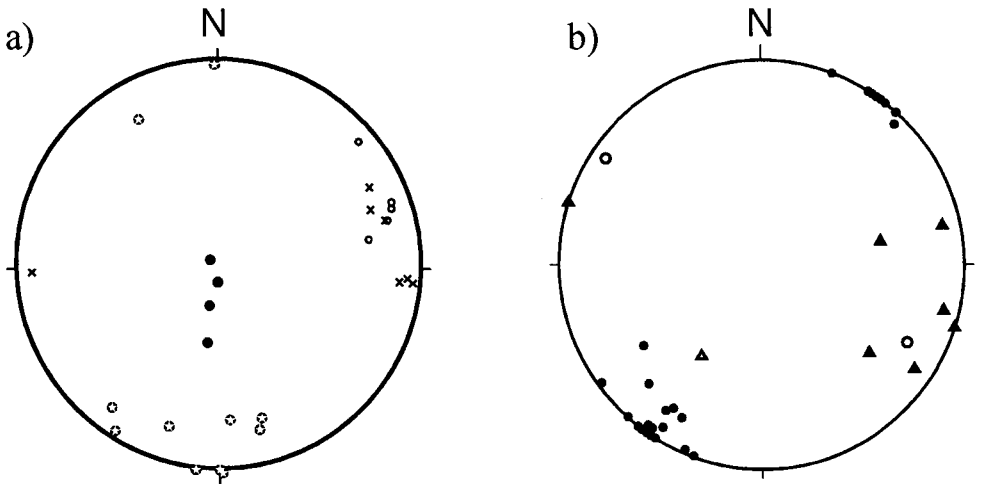

	intrafolial fold	open to gentle fold
Pole to axial surface	●	○
Fold axis	○	×

Sense-of-shear	Fault plane	lineation
dextral	●	○
sinistral	▲	△

Fig. 3. a) Lower hemisphere equal area projection of poles to axial surfaces and fold axis of earlier folds (intrafolial folds) and later folds (upright folds). b) Geometry and sense-of-shear in narrow mylonite zones.

parallel to the high-strain zones (Plate 2-4e). Some mylonite zones are composed of obliquely-foliated central parts and marginal parts of biotite-rich ultramylonite (Plate2-4f). Foliation in the ultramylonite margins is parallel to the mylonite zone. Narrow mylonite zones show various kinds of asymmetric structures such as asymmetric drag folds (deflection of foliation), S-C structures (Lister and Snoke, 1984), porphyroclasts with asymmetric tails of recrystallized matrix minerals, and oblique grain-shape foliations in recrystallized aggregates. The asymmetric structures indicate that the NW-SE and N-S trending mylonite zones were produced by shearing in dextral and sinistral senses respectively (Fig. 3b and Plates 2-4e and f). The orientations of the principal stress axes were preliminarily determined in the conjugate fault set as follows:

σ 1 (maximum compressive stress) is NNW-SSE to NW-SE,
σ 2 (intermediate principal stress) is nearly vertical,
σ 3 (minimum principal stress) is ENE-WSW to NE-SW .

6. Geochemistry

Representative chemical analyses for the metamorphic and intrusive rocks from Skallen are listed in Tables 2 and 3, respectively. Sample localities of the analytical data are marked on the geological map.

Table 2. Representative chemical analyses for metamorphic rocks from Skallen.

Sample No.	C9712	9501	C9712	C9712	C9712	C9712	C9712	C9712	C9712	C9712	9501
	2001D	2705	2103B	2601B	2201A	2203B	1901B	2001B	2004A	2401E	2801
Rock name	Amph	Amph	Opx-Hbl gn	Grt-Opx amph	Hbl gn	Granitic gn	Grt-Bt gn	Grt-Bt gn	Grt-Sil gn	Grt-Opx gn	Anatexite
SiO_2 (wt%)	45.72	40.89	47.03	51.91	71.03	65.84	74.18	71.34	63.90	48.84	72.40
TiO_2	1.94	3.16	1.45	3.31	0.58	0.61	0.46	0.45	1.67	1.29	0.25
Al_2O_3	15.90	13.16	16.15	13.65	13.23	17.03	13.24	13.73	15.22	13.48	15.33
Fe_2O_3*	14.30	14.57	13.13	17.83	4.76	3.14	2.84	3.94	9.92	16.03	1.43
MnO	0.18	0.20	0.18	0.28	0.08	0.02	0.02	0.06	0.14	0.21	0.43
MgO	7.54	10.99	8.69	3.47	0.60	1.56	0.72	0.80	3.11	6.89	0.01
CaO	9.61	11.66	9.32	6.85	2.50	4.33	2.07	2.02	2.21	11.15	1.52
Na_2O	2.68	2.35	3.00	1.84	2.38	3.95	3.11	2.37	2.15	2.06	3.11
K_2O	1.96	1.58	1.31	0.45	4.53	2.26	2.93	5.10	1.77	0.87	5.73
P_2O_5	0.16	0.44	0.10	0.54	0.09	0.12	0.05	0.12	0.04	0.08	0.11
Total	99.98	99.00	100.36	100.15	99.78	98.85	99.61	99.93	100.12	100.89	100.32
Ba (ppm)	124	630	171	136	2284	738	847	1380	825	73	1665
Cr	118	143	121	100	4	8	10	12	276	97	6
Nb	7	16	4	35	15	7	5	10	25	7	6
Ni	130	79	180	41	7	17	10	9	145	88	7
Rb	117	36	74	38	141	116	131	213	52	49	64
Sr	274	374	265	90	335	471	350	228	236	79	287
V	297	305	239	432	55	74	59	54	290	392	24
Y	44	47	28	176	53	7	10	46	62	41	2
Zn	128	211	93	198	40	52	42	40	147	148	28
Zr	112	247	92	419	375	8	196	224	323	78	76
X_{Mg}	0.51	0.60	0.57	0.28	0.20	0.50	0.33	0.29	0.38	0.46	0.01
ASI	0.66	0.49	0.69	0.85	0.99	1.01	1.10	1.05	1.61	0.55	1.09

Total Fe as Fe_2O_3. X_{Mg}: Mg/(Fe+Mg) [mol]. ASI: $Al_2O_3/(CaO+Na_2O+K_2O)$ [mol].

Table 3. Representative chemical analyses for granitic rocks from Skallen.

Sample No.	95012701	95012803	95012804	95012703	95012704	95012805	95012806	95012807	95013001	C97122802C
Rock Name	Bt granite	Bt granite	Bt granite	Bt tonalite	Bt tonalite	Bt tonalite	Bt tonalite	Bt tonalite	Bt tonalite	Ms-Bt granite
Occurrence	sheet	sheet	sheet	pod	pod	pod	pod	pod	pod	dike
SiO_2(wt%)	70.88	72.08	70.46	75.80	76.54	79.66	67.43	74.70	73.26	69.78
TiO_2	0.01	n.d.	0.12	0.41	0.36	0.07	0.22	0.02	0.17	1.67
Al_2O_3	16.45	15.81	16.72	11.61	12.69	12.60	18.96	15.21	16.18	13.92
Fe_2O_3	0.14	0.08	0.51	2.80	1.67	0.66	1.26	0.21	0.70	4.48
MgO	n.d.	0.08	0.22	0.14	0.34	0.23	0.60	0.07	0.36	0.01
MnO	n.d.	n.d.	0.01	0.02	0.01	0.02	0.01	0.01	0.01	1.16
CaO	1.07	0.39	1.70	1.91	2.62	3.30	4.02	1.91	4.14	2.72
Na_2O	3.10	2.25	2.85	2.55	3.84	2.97	5.44	3.68	4.02	2.57
K_2O	8.46	9.78	7.36	2.94	0.73	0.70	1.46	4.62	1.07	4.50
P_2O_5	0.01	0.02	0.01	0.03	0.03	0.00	0.19	0.00	0.01	0.15
L.O.I.	0.26	0.23	0.24	1.33	0.98	0.26	0.59	0.24	0.39	n.d.
Total	100.38	100.72	100.20	99.53	99.81	100.47	100.18	100.67	100.31	100.96
As (ppm)	2	1	n.d.	2	4	n.d.	3	4	n.d.	n.d.
Ba	1415	1314	1494	933	133	163	320	324	456	2232
Ce	6	8	9	107	69	7	25	1	23	n.d.
Cr	4	2	4	3	2	4	6	3	5	4
Cu	30	2	5	12	15	4	247	8	16	n.d.
Ga	14	17	21	9	14	11	15	13	18	n.d.
La	2	7	2	53	35	7	13	n.d.	16	n.d.
Nb	3	2	2	13	13	2	4	2	3	7
Ni	6	7	6	4	4	1	8	4	3	24
Pb	8	85	20	9	76	10	58	87	19	n.d.
Rb	82	158	50	36	276	13	247	321	21	139
Sc	n.d.	n.d.	2	7	9	3	2	1	2	n.d.
Sr	68	112	322	99	246	217	253	183	488	435
Th	19	2	2	5	2	2	2	1	2	n.d.
V	5	4	22	10	14	11	29	5	22	102
Y	12	n.d.	n.d.	111	n.d.	3	n.d.	n.d.	n.d.	21
Zn	n.d.	n.d.	9	18	13	3	45	n.d.	10	73
Zr	15	12	18	380	345	25	178	20	312	538
Na_2O+K_2O	11.56	12.03	10.21	5.49	4.57	3.67	6.90	8.30	5.09	7.07
K_2O/Na_2O	2.73	4.35	2.58	1.15	0.19	0.24	0.27	1.26	0.27	1.75
ASI	1.02	1.05	1.06	1.07	1.07	1.08	1.06	1.05	1.06	0.99

Total Fe as Fe_2O_3. X_{Mg}: Mg/(Fe+Mg) [mol]. ASI: $Al_2O_3/(CaO+Na_2O+K_2O)$ [mol]. n.d.: not determined.

Mafic rocks including amphibolite (95012705, C97122001D), orthopyroxene-bearing hornblende gneiss (C97122103B) and garnet-orthopyroxene hornblende gneiss (C97122601B) with 40 to 52 wt% SiO_2 and high concentrations of Fe_2O_3 (14-18 wt%) relative to MgO (3-11 wt%), indicating a tholeiitic signature. Amphibolite and orthopyroxene-bearing hornblende gneiss have relatively high K_2O, reflecting the presence of biotite.

Quartzo-feldspathic gneiss (garnet-biotite gneiss: C97121901B, C97122001B) and hornblende gneiss (C97122201A) have similar SiO_2 contents (71 to 74 wt%). Alumna-saturation index (ASI) values have a positive correlation with increasing SiO_2. Hornblende gneiss has a metaluminous signature. Garnet-sillimanite gneiss (C97122004A) possesses moderate SiO_2 (64 wt%) with high ASI value (1.6). Garnet-orthopyroxene granulite (C97122401E) is enriched in Fe_2O_3, CaO and depleted in K_2O, Rb, with low concentrations of SiO_2. The ASI value is very low (0.55). These

geochemical features suggest that garnet-orthopyroxene granulite is derived from a tholeiitic cumulate or a restite of a mafic protholith after release of granitic melt.

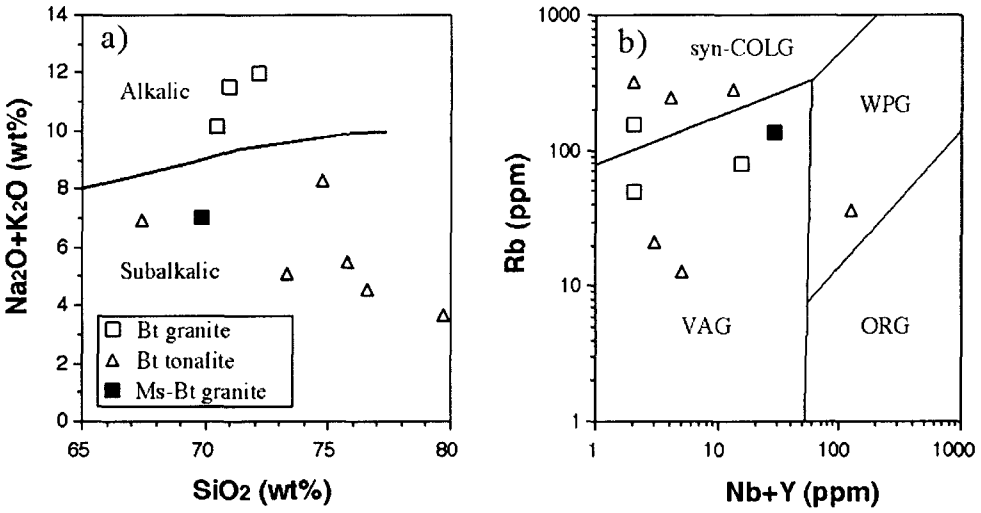

Fig. 4. a) Total alkali (Na_2O+K_2O wt%) versus SiO_2 (wt%) (TAS diagram). The chemical classification of alkalic and subalkalic rocks is after Cox et al. (1979), as adapted by Wilson (1989) for plutonic rocks. b) Rb (ppm) versus Nb+Y (ppm) diagram for granite (after Pearce et al., 1984) showing the fields of syn-collisional granite (syn-COLG), within-plate granite (WPG), volcanic-arc granite (VAG) and oceanic-ridge granite (ORG).

Granitic gneiss would originally be igneous as previously described, and has moderate SiO_2 (66 wt%) with relatively high concentrations of Al_2O_3, Na_2O and Sr. Values of K_2O and Y are low (2.26 wt% and 7 ppm). The geochemical character of the granitic gneiss is similar to that of high-Al TTG reported from world wide, as well as meta-trondhjemite from Cape Hinode described by Shiraishi *et al.* (1995) and Ikeda *et al.* (1997).

Anatexite occurs as small lenses in various kinds of gneiss, and is leucocratic to pinkish in color. It has 72 wt% SiO_2 and a peraluminous signature (ASI=1.09), and also moderate K_2O (5.70 wt%) and Ba (1665 ppm), reflecting the presence of K-feldspar (55.3 modal %).

The granitic rocks have been divided geologically and petrographically into three types: biotite tonalite, biotite granite and muscovite-biotite granite. Biotite granite intruded as sheets and shows higher K_2O/Na_2O ratios than biotite tonalite, which occurs as pods in the host gneiss, reflecting modal variation of K-feldspar. The muscovite-biotite granite dike has a moderate K_2O/Na_2O ratio.

Figure 4 shows total alkali *versus* SiO_2 (Wilson, 1989) and Rb *versus* Nb+Y (Pearce *et al.*, 1984) for the three types of granite. All types of granite have 67 to 80 wt% SiO_2. Biotite granite falls within the field of alkalic rocks, whereas other two

types of granite show sub-alkalic signatures (Fig. 4a). On the Rb *versus* Nb+Y diagram, biotite tonalite is characterized by a wide compositional range across the syn-COLG, VAG and WPG fields, whereas biotite granite falls within syn-COLG and VAG with a narrow variation (Fig. 4b). Muscovite-biotite granite has the geochemical signature of VAG. ASI values of the three types of granite are less than 1.1, and are I-type granites (Chappell and White, 1974), although some contain peraluminous minerals such as garnet and muscovite, and show wide geochemical variations. The formation of granitic magma would, therefore, not been derived directly from the pelitic gneisses exposed at Skallen.

7. Metamorphic conditions and evolution

Prior to Yoshida *et al.* (1976), Banno *et al.* (1964) identified the regional metamorphism of the Lützow-Holm Bay region including Skallen as belonging to the granulite-facies, based on the common occurrence of orthopyroxene in basic to intermediate rocks, TiO_2-rich biotite and MgO-rich garnet in metapelitic rocks. Metastable kyanite and staurolite were first found in garnet-sillimanite gneiss from Skallen by Y. Hiroi and their modes of occurrence were reported by Motoyoshi *et al.* (1985). These relict minerals occuring as inclusions in garnet suggest that the basement rocks in the region have been subjected to prograde metamorphism that progressed from the kyanite field to the sillimanite field. This petrographical evidence is peculiar amongst high-grade metamorphic terranes in the East Antarctic Shield, as no obvious prograde *P-T* paths have been reported except for the Lützow-Holm Complex (*e.g.* Harley and Hensen, 1990). In addition to the prograde history mentioned above, Hiroi *et al.* (1991) revealed a progressive change in metamorphic grade from the amphibolite-facies terrane in the east to the granulite-facies terrane in the southwest. Skallen is located close to the thermal axis of the Lützow-Holm Complex.

Metamorphic *P-T* conditions have been estimated by means of various geothermobarometries by the following workers:

Yoshida and Aikawa (1983): 823°C, 4.1-6.5 kbar,

Suzuki (1983): 725 ± 25°C, 6.3 ± 1.3 kbar,

Motoyoshi (1986): 810°C, 7.7-10.8 kbar.

Newly calculated metamorphic temperatures for mafic granulite (B97122603B) using garnet-orthopyroxene (Harley, 1984; Lee and Ganguly, 1988; Pattison *et al.*, 2003), garnet-clinopyroxene (Ellis and Green, 1979; Powell, 1985; Pattison and Newton, 1989; Ravna, 2000), garnet-hornblende (Graham and Powell, 1984), and hornblende-plagioclase (Holland and Blundy, 1994) geothermometers are summarized in Table 4. Temperatures obtained by conventional Fe-Mg exchange geothermometers are mostly less than 800°C, and may indicate closure temperatures of cation exchange between mineral pairs. On the other hand, a very high temperature estimate of >1000°C was obtained by the method of Pattison *et al.* (2003), which is a revised garnet-orthopyroxene geothermometer corrected for retrograde exchange between garnet and orthopyroxene. This result might suggest that the Skallen area has undergone much higher temperatures at the peak metamorphism, possibly close to ultrahigh-temperature

conditions. Ikeda (2004) reported 5.6 kbar at 760°C to 6 kbar at 660°C for the retrograde stage conditions.

Table 4. Conventional geothermometries for garnet-bearing two-pyroxene-hornblende gneiss from Skallen (Tsunogae, unpublished data).

sample: B97122603B	T°C (at 8 kbar)
garnet-orthopyroxene	
Harley (1984)	630-720
Lee & Ganguly (1988)	770-870
Pattison *et al.* (2003)	1030
garnet-clinopyroxene	
Ellis & Green (1979)	740-790
Powell (1985)	720-770
Pattison & Newton (1989)	660-720
Ravna (2000)	690-750
garnet-hornblende	
Graham & Powell (1987)	680-740
hornblende-plagioclase	
Holland & Blundy (1994)	740-810

8. Geochronology

The age of granulite/amphibolite facies metamorphism in the Lützow-Holm Complex, including the Skallen area, has been well constrained as Pan-African (*c.* 550-520 Ma) by SHRIMP U-Pb zircon analysis (*e.g.*, Shiraishi *et al.*, 1994, 2003; Fraser *et al.*, 2000). Most Sm-Nd whole rock isochron ages, K-Ar hornblende ages and electron microprobe monazite (CHIME) ages fall within the same age bracket (Asami *et al.*, 1997; Nishi *et al.*, 2002; and the references therein). Combined SHRIMP zircon analyses and Ar-Ar hornblende and biotite chronology by Fraser *et al.* (2000) suggested that the post-peak decompression and subsequent cooling to *c.* 300-350°C took place within a time interval of *c.* 520-500 Ma. A few Rb-Sr and Sm-Nd whole-rock isochron ages give slightly older *c.* 700-600 Ma ages (*e.g.*, Nishi *et al.*, 2002). Similar ~*c.* 600 Ma ages, slightly older than 550-520 Ma peak metamorphic event, has also been reported from the Yamato-Belgica Complex (Shiraishi *et al.*, 2003). However, it is not clear if these older ages reflect the metamorphic event, magmatic protolith ages, or partial isotopic resetting. The ages of protolith formation for gneisses in the Lützow-Holm Complex are not well understood. SHRIMP analyses on zoned zircon cores of trondhjemite from Cape Hinode yielded *c.* 1000 Ma Grenvillian ages, which are interpreted as igneous protolith ages (Shiraishi *et al.*, 2003). Sedimentary precursors to some of the paragneisses suggest inherited zircon core ages as old as Proterozoic to Archaean analyzed by SHRIMP; this suggests that older materials comprise the protoliths of the Lützow-Holm Complex; thus the Lützow-Holm Complex is considered to be a collage of pre-Grenvillian continental blocks and Grenvillian juvenile crust amalgamated by the Pan-African convergence (Shiraishi *et al.*, 2003).

Table 5. Ages of metamorphic and igneous rocks from Skallen.

Method	Rock type	Age	Sample No.	Ref.
Rb-Sr biotite	pegmatite	525 ± 40 Ma	57112001	1
	pegmatite	530 ± 16 Ma	57102622	1
	pegmatite	510 ± 30 Ma	57110704	1
	pegmatite	500 ± 30 Ma	57122307	1
U-Pb euxenite	pegmatite	*c.* 470 Ma (458 ± 21 ~ 485 ± 6 Ma)	not shown	2
U-Th-total Pb monazite	Quartzo-feldspathic garnet-biotite gneiss	539 ± 15 Ma	A97122303A	3
	Quartzo-feldspathic garnet-biotite gneiss	543 ± 14 Ma	A97122303B	3

1: Nicolaysen *et al.* (1961), 2: Saito *et al.* (1961), 3: Hokada (unpublished data)

Geochronological data from the Skallen area are summarized in Table 5. Nicolaysen *et al.* (1961) reported *c.* 530-500 Ma ages by Rb-Sr biotite analysis, and younger *c.* 470 Ma (U-Pb) ages were reported for euxenite in granitic pegmatite (Saito *et al.*, 1961). Monazite U-Th-Pb chemical ages analyzed by electron microprobe for garnet-biotite-bearing quartzo-feldspathic gneiss yielded 539 ± 15 Ma and 543 ± 14 Ma (Hokada, unpublished data). These data are mostly consistent with the *c.* 550-520 Ma (Pan-African) metamorphic event in the Lützow-Holm Complex. No older inheritance or protolith ages have been reported from this area.

Acknowledgments

We express our thanks to K. Hasegawa and K. Seno for editorial assistance, and to D. J. Dunkley for improving English in the text.

References

Asami, M., Suzuki, K. and Adachi, M. (1997): Th, U and Pb analytical data and CHIME dating of monazites from metamorphic rocks of the Rayner, Lützow-Holm, Yamato-Belgica and Sør Rondane Complexes, East Antarctica. Proc. NIPR Symp. Antarct. Geosci., **10**, 130-152.

Banno, S., Tatsumi, T., Kuno, H. and Katsura, T. (1964): Mineralogy of granulite facies rocks in the area around Lützow-Holm Bay, Antarctica. JARE Sci. Rep., Ser. C, **1**, 12 p.

Chappell, B.W. and White, A.J.R. (1974): Two contrasting granite types. Pacific Geol., **8**, 173-174.

Cox, K.G., Bell, J.D. and Pankhurst, R.J. (1979): The Interpretation of Igneous Rocks. London, George Allen and Unwin, 450 p.

Ellis, D.J. and Green, D.D. (1979): An experimental study of the effect of Ca upon garnet-clinopyroxene Fe-Mg exchange equilibria. Contrib. Mineral. Petrol., **71**, 13-22.

Fraser, G., McDougall, I., Ellis, D.J. and Williams, I.S. (2000): Timing and rate of isothermal decompression in Pan-African granulites from Rundvågshetta, East Antarctica. J. Metamor. Geol., **18**, 441-454.

Graham, C.M. and Powell, R. (1984): A garnet-hornblende geothermometer: calibration, testing, and application to Pelona Schist, Southern California. J. Metamor. Geol., **2**, 13-31.

Harley, S.L. (1984): An experimental study of the partitioning of Fe and Mg between garnet and orthopyroxene. Contrib. Mineral. Petrol., **86**, 359-373.

Harley, S.L. and Hensen, B.J. (1990): Archaean and Proterozoic high-grade terranes of East Antarctica (40-80°E): A case study of diversity in granulite facies metamorphism. High Temperature Metamorphism and Crustal Anatexis, ed. by J.R. Ashworth and M. Brown. London, Unwin

Hyman, 320-370.
Hiroi, Y., Shiraishi, K. and Motoyoshi, Y. (1991): Late Proterozoic paired metamorphic complexes in East Antarctica, with special reference to the tectonic significance of ultramafic rocks. Geological Evolution of Antarctica, ed. by M.R.A. Thomson *et al.* Cambridge. Cambridge Univ. Press, 83-87.
Holland, T.J.B. and Blundy, J.D. (1994): Non-ideal interactions in calcic amphiboles and their bearing on amphibole-plagioclase thermometry. Contrib. Mineral. Petrol., **116**, 433-447.
Igarashi, A., Numanami, H., Tsuchiya, Y., Harada, N., Fukuchi, M. and Saito, T. (1995): Radiocarbon ages of molluscan shell fossils in raised beach deposits along the east coast of Lützow-Holm Bay, Antarctica, determined by accelerator mass-spectrometry. Proc. NIPR Symp. Polar Biol., **8**, 154-162.
Ikeda, T. (2004): Garnet-biotite geothermometry of a pelitic gneiss from the Lützow-Holm Complex in Skallen, East Antarctica: constaints on retrograde metamorphism. Submitted to Polar Geosci.
Ikeda, Y., Shiraishi, K. and Yanai, K. (1997): Petrogenesis of the meta-trondhjemites from Cape Hinode, East Antarctica. Proc. NIPR Symp. Antarct. Geosci., **10**, 102-110.
Kusachi, I., Osanai, Y., Toyoshima, T., Owada, M., Tsunogae, T., Hokada, T. and Crowe, W.A. (1999): Mineralogy of scapolite from Skallen in the Lützow-Holm Bay region, East Antarctica. Polar Geosci., **12**, 143-156.
Leake, B.E., Woolley, A.R., Arps, C.E.S., Birch, W.D., Gilbert, M.C., Grice, J.D., Hawthorne, F.C., Kato, A., Kisch, H.J., Krivovichev, V.G., Linthout, K., Laird, J., Mandarino, J.A., Maresch, W.V., Nickel, E.H., Rock, N.M.S., Schumacher, J.C., Smith, D.C., Stephenson, N.C.N., Ungaretti, L., Whittaker, E.J.W. and Youzhi, G. (1997): Nomenclature of amphiboles: Report of the subcommittee on amphiboles of the International Mineralogical Association, commission on new minerals and mineral names. Am. Mineral., **82**, 1019-1037.
Lee, H.Y. and Ganguly, J. (1988): Equilibrium compositions of coexisting garnet and orthopyroxene: experimental determinations in the system FeO-MgO-Al_2O_3-SiO_2, and applications. J. Petrol., **29**, 93-113.
Lister, G. S. and Snoke, A. W. (1984): S-C mylonites. J. Struct. Geol., **6**, 617-638.
Michibayashi, K., Okamoto, A., Masuzawa, T., Kawakami, T., Ikeda, T., and Yasuda, H. (2004): Orientation contrast images of garnet in granulite-facies quartzite, Lützow-Holm Complex, East Antarctica. J. Geol. Soc. Jpn., **110**, No. 3, v-vi (pictorial).
Motoyoshi, Y. (1986): Prograde and progressive metamorphism of the granulite-facies Lützow-Holm Bay region, East Antarctica. PhD Thesis, Hokkaido Univ., 238 p.
Motoyoshi, Y., Matsubara, S., Matsueda, H. and Matsumoto, Y. (1985): Garnet-sillimanite gneisses from the Lützow-Holm Bay region, East Antarctica. Mem. Natl Inst. Polar Res., Spec. Issue, **37**, 127-146.
Nicolaysen, L.O., Burger, A.J., Tatsumi, T. and Ahrens, L.H. (1961): Age measurements on pegmatites and a basic charnockite lens occurring near Lützow-Holm Bay, Antarctica. Geochim. Cosmochim. Acta, **22**, 94-98.
Nishi, N., Kawano, Y. and Kagami, H. (2002): Rb-Sr and Sm-Nd isotopic geochronology of the granitoid and hornblende biotite gneiss from Oku-iwa Rock in the Lützow-Holm Complex, East Antarctica. Polar Geosci., **15**, 46-65.
Omoto, K. (1977): Geomorphic development of the Sôya Coast, East Antarctica - Chronological interpretation of raised beaches based on levellings and radiocarbon datings. Sci. Rep. Tohoku Univ., 7th Ser. (Geography), **27**, 95-148.
Pattison, D.R.M. and Newton, R.C. (1989): Reversed experimental calibration of the garnet-clinopyroxene Fe-Mg exchange geothermometer. Contrib. Mineral. Petrol., **101**, 87-103.
Pattison, D.R.M., Chacko, T., Farquhar, J. and McFarlane, C.R.M. (2003): Temperatures of granulite-facies metamorphism: constraints from experimental phase equilibria and thermobarometry corrected for retrograde exchange. J. Petrol., **44**, 867-900.
Pearce, J.A., Harris, N.B.W. and Tindle, A.G. (1984): Trace element discrimination diagrams for the tectonic interpretation of granitic rocks. J. Petrol., **25**, 956-983.
Powell, R. (1985) Regression diagnostics and robust regression in geothermometer/geobarometer calibration: the garnet-clinopyroxene geothermometer revisited. J. Metamor. Geol., **3**, 231-243.
Ravna, E.K. (2000): The garnet-clinopyroxene Fe^{2+}-Mg geothermometer: an updated calibration. J. Metamor. Geol., **18**, 211-219.
Saito, N., Tatsumi, T. and Sato, K. (1961): Absolute age of euxenite from Antarctica. Nankyoku Shiryô (Antarct. Rec.), **12**, 31-36.
Sawagaki, T. and Hirakawa, K. (1997): Erosion of bedrock by subglacial meltwater, Sôya Coast, East Antarctica. Geogr. Ann., **79**, 223-238.
Sawagaki, T. and Hirakawa, K. (2002a): Terrestial evidence of melting of the Antarctic Ice Sheet during the last glacial period. R. Soc. N. Z. Bull., **35**, 405-414.
Sawagaki, T. and Hirakawa, K. (2002b): Hydrostatic investigations on subglacial meltwater: implications for the formation of streamlined bedforms and subglacial lakes, East Antarctica. Polar Geosci.,

15, 123-147.
Shiraishi, K., Ellis, D.J., Hiroi, Y., Fanning, C.M., Motoyoshi, Y. and Nakai, Y. (1994): Cambrian orogenic belt in East Antarctica and Sri Lanka: implications for Gondwana assembly. J. Geol., **102**, 47-65.
Shiraishi, K., Hokada, T., Fanning, C.M., Misawa, K. and Motoyoshi, Y. (2003): Timing of thermal events in eastern Dronning Maud Land, East Antarctica. Polar Geosci., **16**, 76-99.
Shiraishi, K., Kagami, H. and Yanai, K. (1995): Sm-Nd and Rb-Sr isochron ages for meta-trondhjemites from Cape Hinode, East Antarctica. Proc. NIPR Symp. Antarct. Geosci., **8**, 130-136.
Suzuki, M. (1983): Preliminary note on the metamorphic conditions around Lützow-Holm Bay, East Antarctica. Mem. Natl Inst. Polar Res., Spec. Issue, **28**, 132-143.
Wilson, M. (1989): Igneous Petrogenesis. London, Unwin Hyman, 466 p.
Yoshida, M. (1977): Geology of the Skallen Region, Lützow-Holmbukta, East Antarctica. Mem. Natl Inst. Polar Res., Ser. C, **11**, 38 p.
Yoshida, M. and Aikawa, N. (1983): Petrography of a discordant metabasite from Skallen, Lützow-Holmbukuka, East Antarctica. Mem. Natl Inst. Polar Res., Spec. Issue, **28**, 144-165.
Yoshida, M., Yoshida, Y., Ando, H., Ishikawa, T. and Tatsumi, T. (1976): Geological Map of Skallen, Antarctica. Antarct. Geol. Map Ser., Sheet **9** (with explanatory text 16p.), Tokyo, Natl Inst. Polar Res.
Yoshida, Y. (1983): Physiography of the Prince Olav and the Prince Harald Coasts, East Antarctica. Mem. Natl Inst. Polar Res., Ser. C, **13**, 83 p.

Plate 1

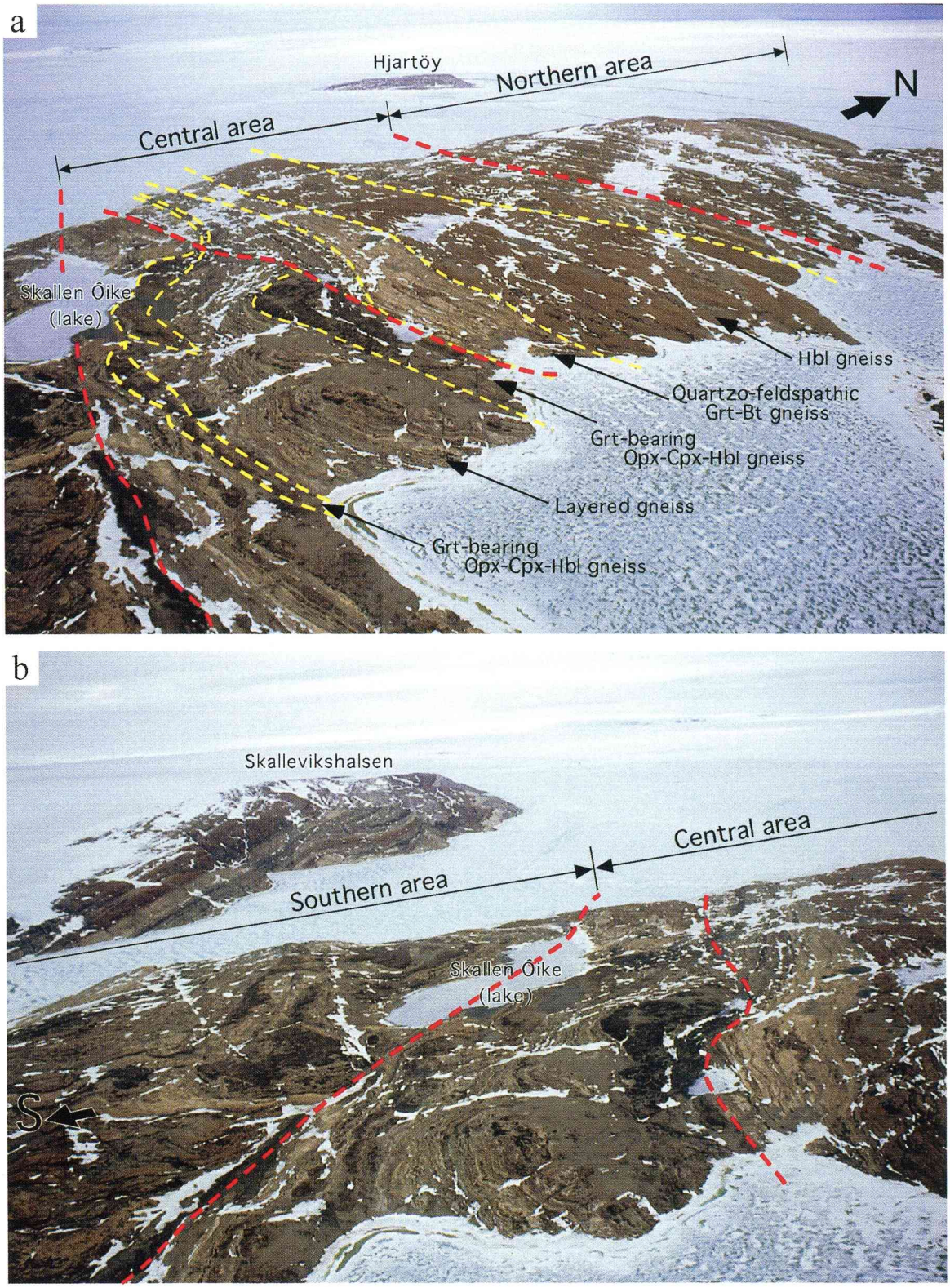

Plate 1. (a) An aerophotogrph of northern and central areas of Skallen, viewed from helicopter flying over SE-coast. Well layering of gneisses and structural disturbances due to the shear zones (red broken lines) are clearly observed. (b) An aerial photograph of southern and central areas of Skallen, viewed from helicopter flying over E-coast. Characteristic meranocratic bodies of mafic metamorphic rocks are observed.

Plate 2-1

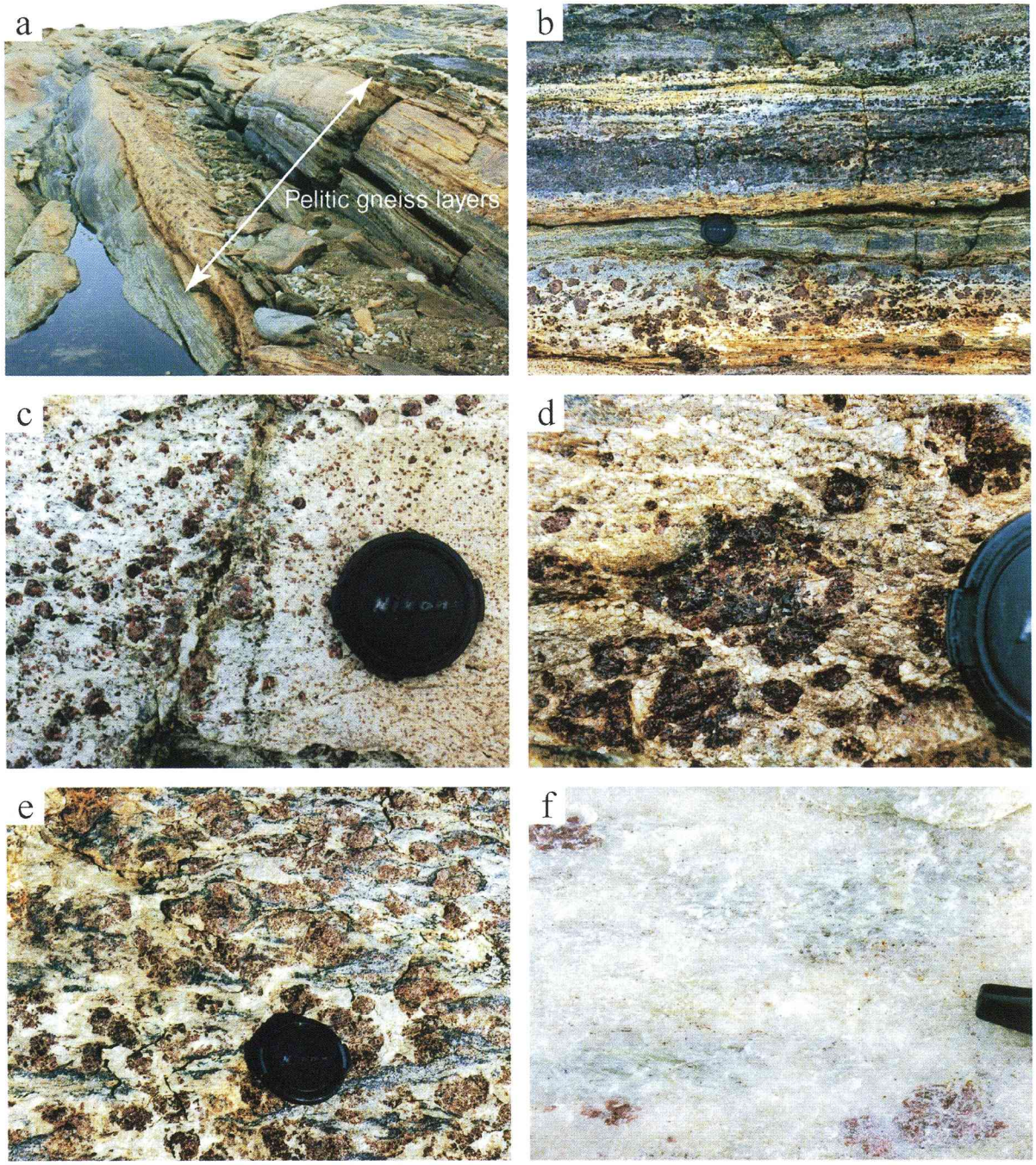

Plate 2-1. Field occurence of pelitic and quartzo-feldspathic rocks. (a) Pelitic gneiss layers occur in alternation of quartzo-feldspathic and mafic gneisses. (b) Pelitic gneiss layers composed of garnet-sillimanite-spinel gneiss, quartzo-feldspathic garnet gneiss and garnet-biotite gneiss. (c) Quartzo-feldspathic garnet gneiss. Grain size of garnet varies. (d) Garnet-orthopyroxene-bearing gneiss occuring as pods. (e) Garnet-sillimanite-spinel gneiss. Dark green-blue spinel is commonly associated with sillimanite or plagioclase. (f) Quartzo-feldspathic garnet-sillimanite gneiss. Whitish appearance is characterized by the rich in quartz-feldspar and poor in biotite.

Plate 2-2

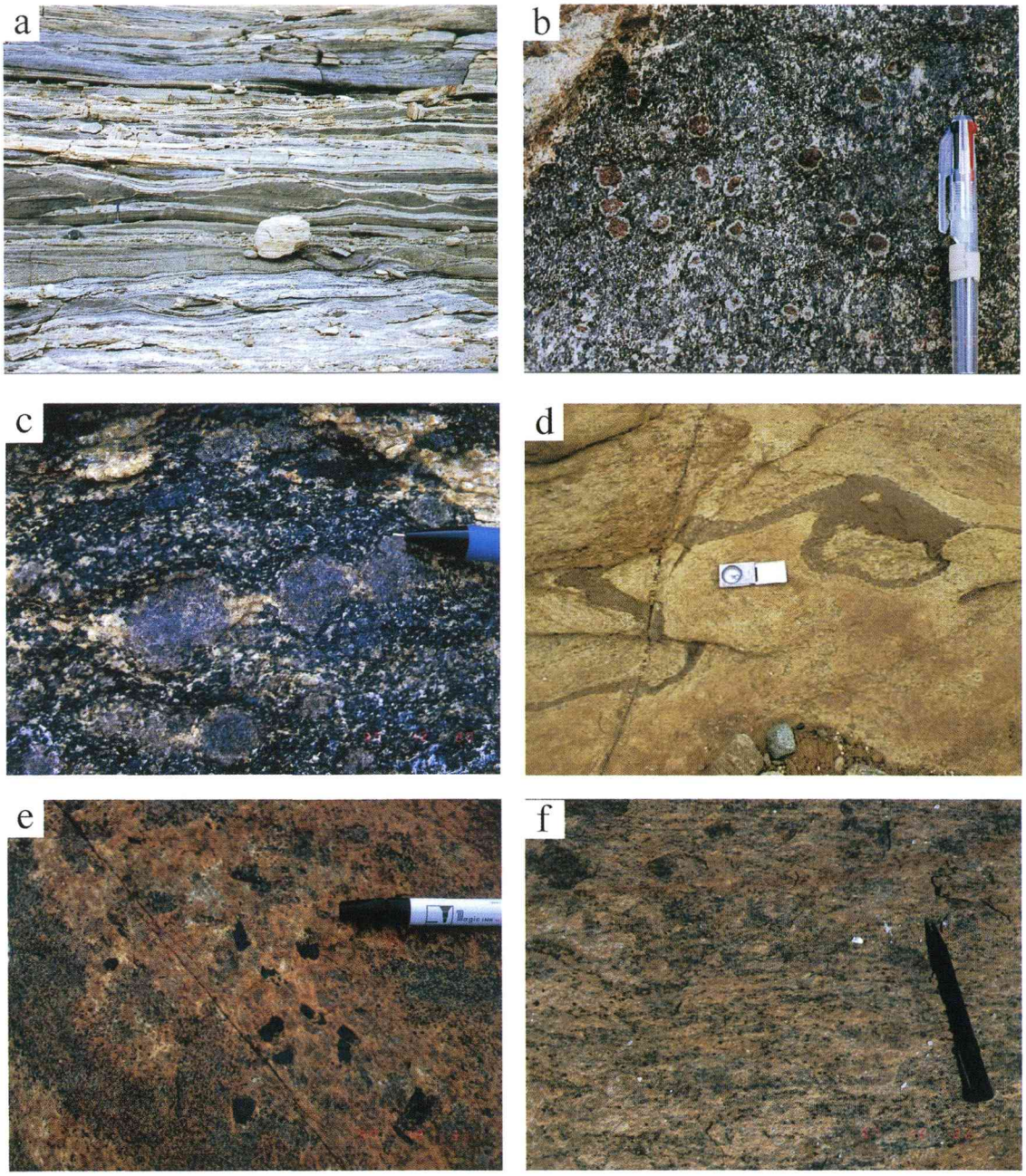

Plate 2-2. (a) Boudins of two-pyroxene-hornblende gneiss elongated parallel to the matrix foliation. (b) Orthopyroxene + plagioclase corona around garnet in two-pyroxene-hornblende gneiss. (c) Spotted aggregates of orthopyroxene + plagioclase in garnet-free two-pyroxene-hornblende mafic gneiss, suggesting consumption of garnet due to the progress of the reaction (1). (d) Two-pyroxene mafic gneiss cutting foliation of matrix quartzo-feldspathic gneiss. (e) Coarse-grained orthopyroxene + plagioclase patches in medium-grained two-pyroxene-hornblende gneiss. (f) Weekly-foliated medium-grained hornblende gneiss (brown gneiss).

Plate 2-3

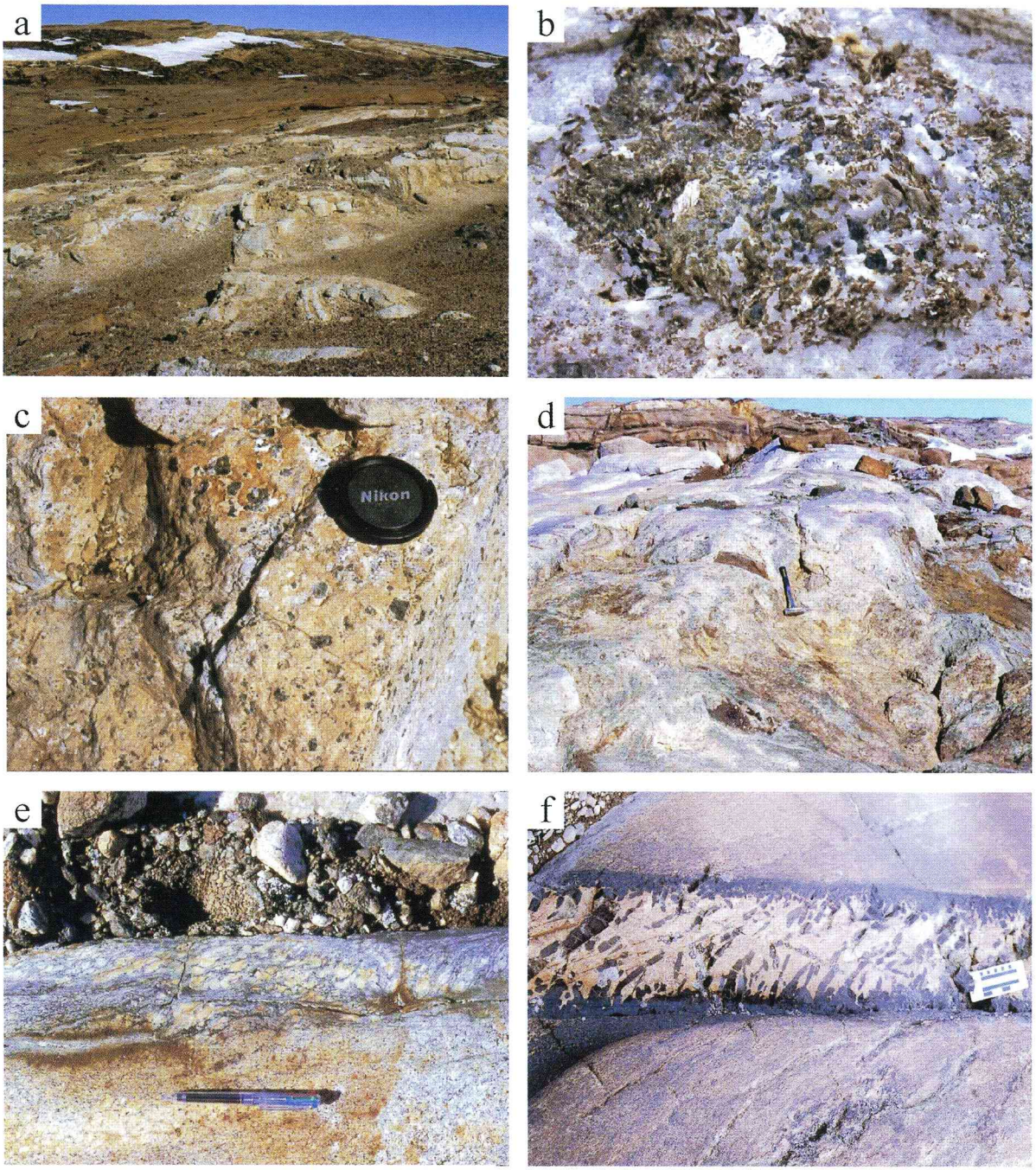

Plate 2-3. (a) Marbles and related calc-silicate bands surrounded by quartzo-feldspathic, pelitic and mafic metamorphic rocks at the southern most part of northern area, which distribute along the areal boundary shear zone. (b) Close up of spinel- and phlogopite-bearing impure marble at the northen end of Skallen. (c) Close up of euhedral- to subhedral-scapolite spotted calc-silicate rock from southern area. (d) Occurrence of granitic gneiss. Note: The granitic gneiss intrudes the garnet-biotite gneiss to form the migmatitic signature at the boundary of the lithologies. (e) The muscovite-biotite granite dike cutting the layers of the host gneisses with chilled margins. Note: the granite dike occurs along the mylonitic shear zone with N-S strike. (f) The pegmatite dike intruding the host gneiss. This pegmatite contains huge hornblende crystals.

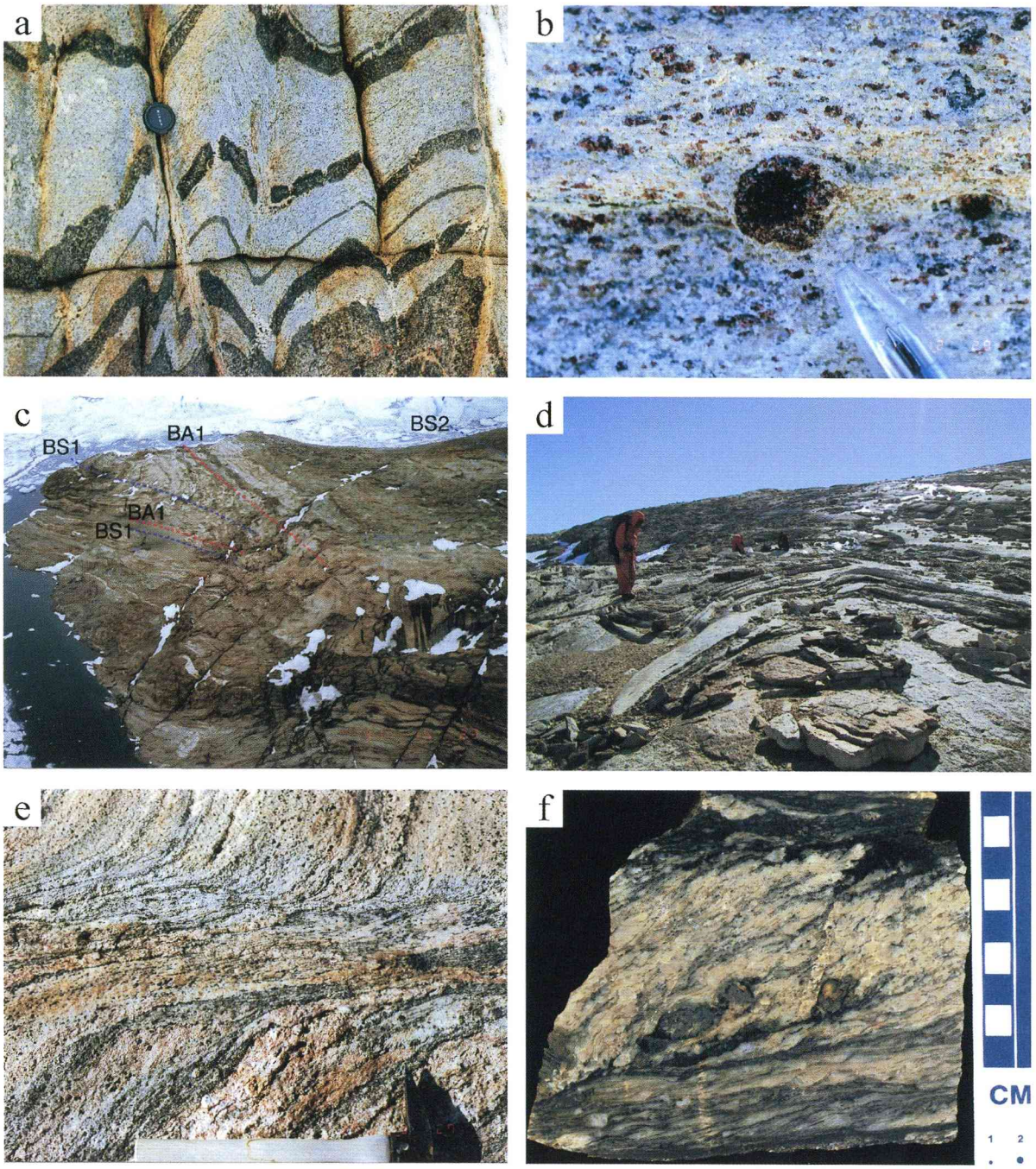

Plate 2-4. Deformation structures found in Skallen. (a) Folded and rotated boudinage of mafic layers, showing layer-parallel shearing and contraction after layer-parallel extension. The intrafolial fold result from top-to-the east shearing. (b) Garnet grain with asymmetric tails containing sillimanite needles, showing top-to-the east shearing. (c) Geological-map scale asymmetric intrafolial folds with ENE-WSW to E-W trend (BS1, BA1), northwest of Osiage Hama (beach), refolded in geological-map scale open to gentle synform (BS2)(top right). (d) Open to gentle upright folds in the northern part. (e) Narrow mylonite zone showing dextral-strike-slip movement. The foliation of the surrounding weakly-mylonitized gneiss is dragged and curves parallel to the high-strain zone. (f) Composed mylonite zone with obliquely-foliated central part and marginal parts of biotite-rich ultramylonite. The foliations of the ultramylonite margins are parallel to the mylonite zone.

Plate 3-1

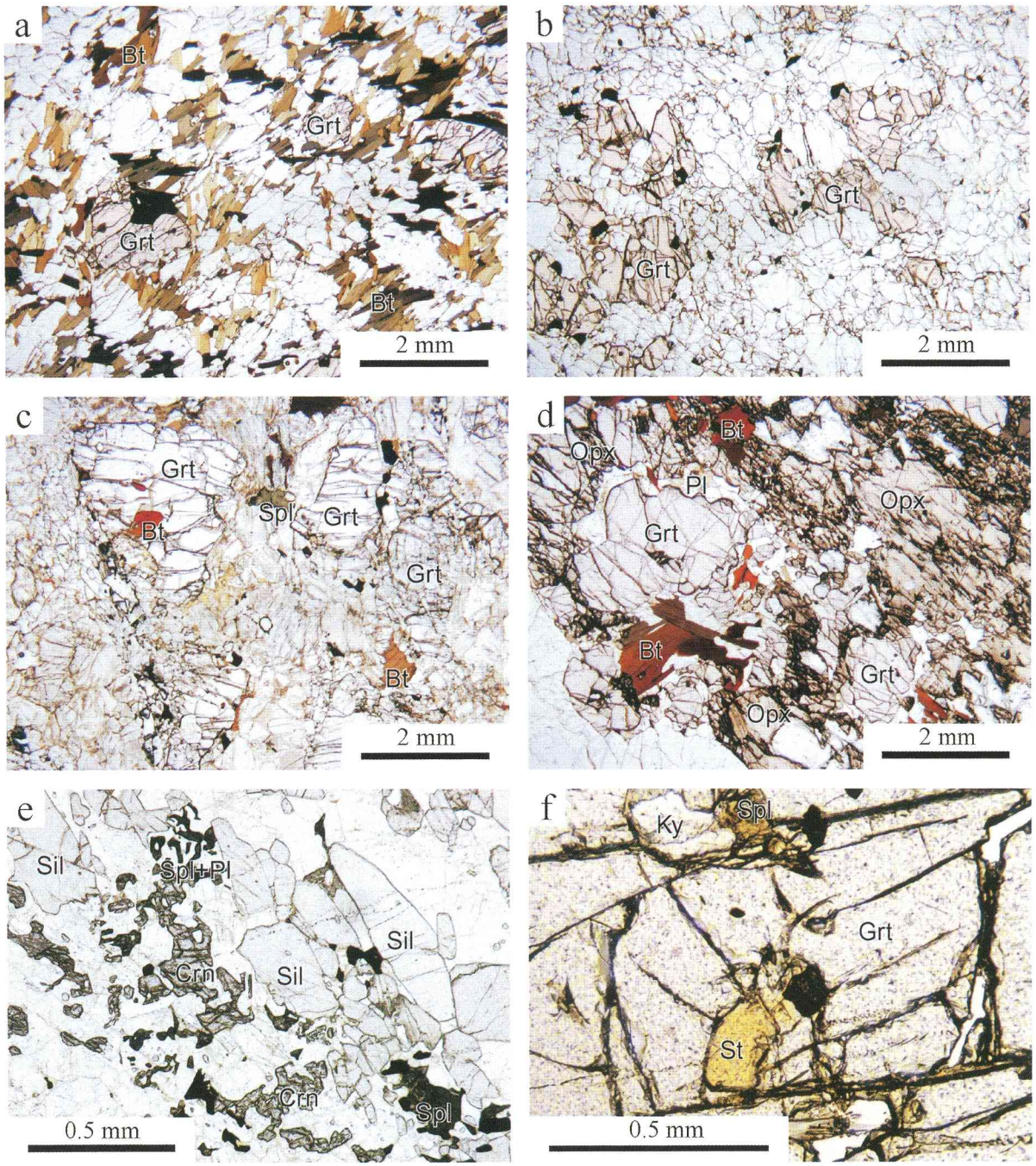

Plate 3-1. Photomicrographs of pelitic and quartzo-feldspathic rocks. Plane-polarized light. (a) Quartzo-feldspathic garnet-biotite gneiss. Aligned sub-idiomorphic biotite grains define a foliation. (b) Quartzo-feldspathic garnet gneiss. Sub-rounded garnet includes rounded quartz and feldspar grains. (c) Garnet-sillimanite-spinel gneiss. Idiomorphic sillimanite grains occur around or as inclusions in garnet. Greenish spinel occurs in asssociation with garnet, sillimanite or plagioclase. (d) Garnet-orthopyroxene-bearing gneiss. Plagioclase crystals occur between garnet and orthopyroxene porphyroblasts. (e) Corundum-spinel-garnet-sillimanite gneiss. (f) Garnet-sillimanite-spinel gneiss. Kyanite and staurolite occur as inclusions in garnet.

Plate 3-2

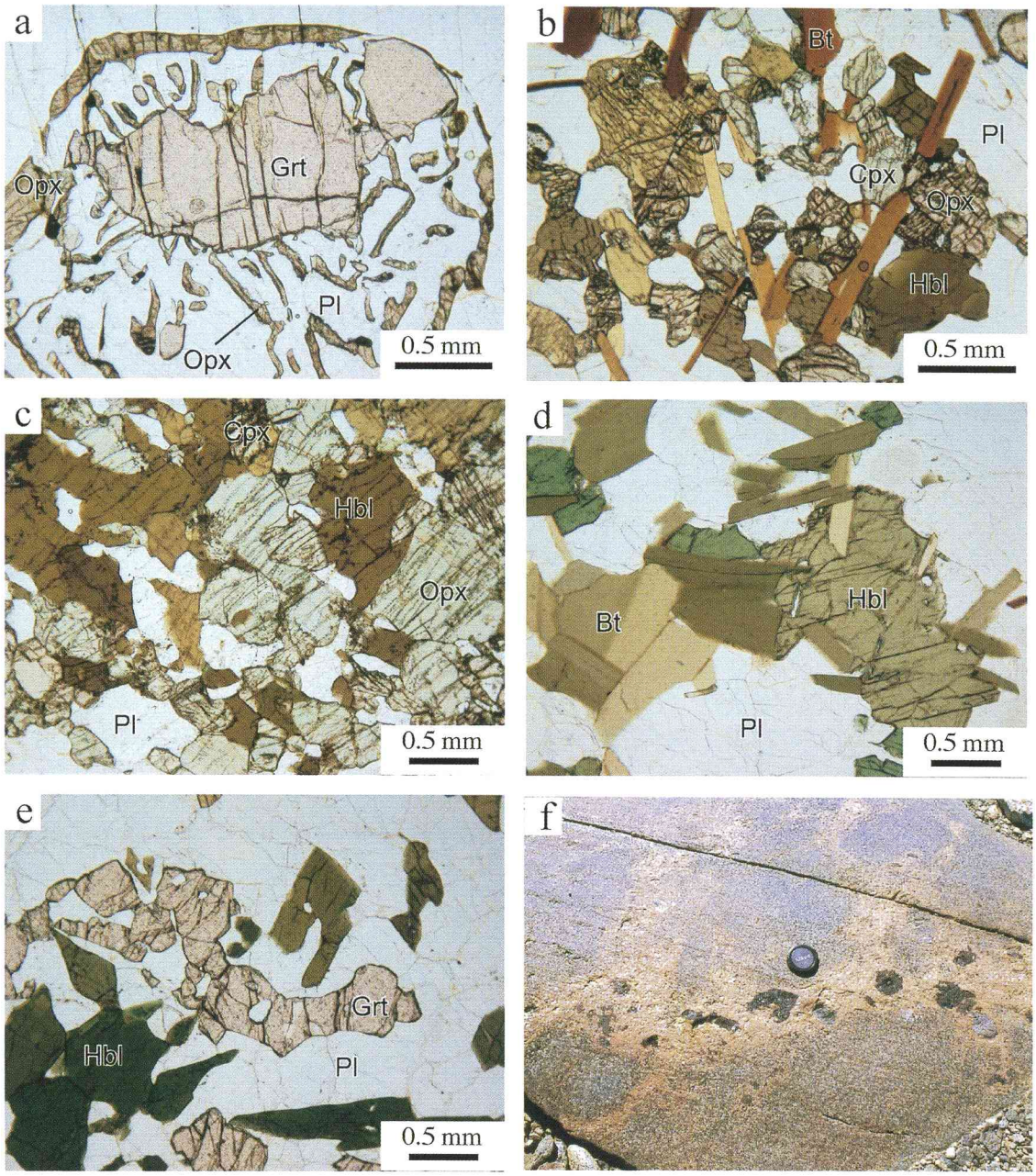

Plate 3-2. Photomicrographs (except field occurrence in Plate 3-2f) showing mineral assemblages of mafic rocks. Plane-polarized light. (a) Orthopyroxene + plagioclase corona around garnet in sample B97122001. (b) Orthopyroxene-hornblende-biotite assemblage in sample B97122404B. (c) Biotite-free orthopyroxene-hornblende assemblage in sample B97122404B. (d) Coarse-grained hornblende-biotite assemblage in brown gneiss (sample B97122702C). (e) Garnet-bearing variety of hornblende gneiss (brown gneiss). (f) Large euhedral crystals of orthopyroxene in anhydrous tonalitic vein, representing a melt segregation derived from incongruent partial melting of hornblende-bearing two pyroxene mafic granulite at Skallen Ôike (lake).

Plate 3-3

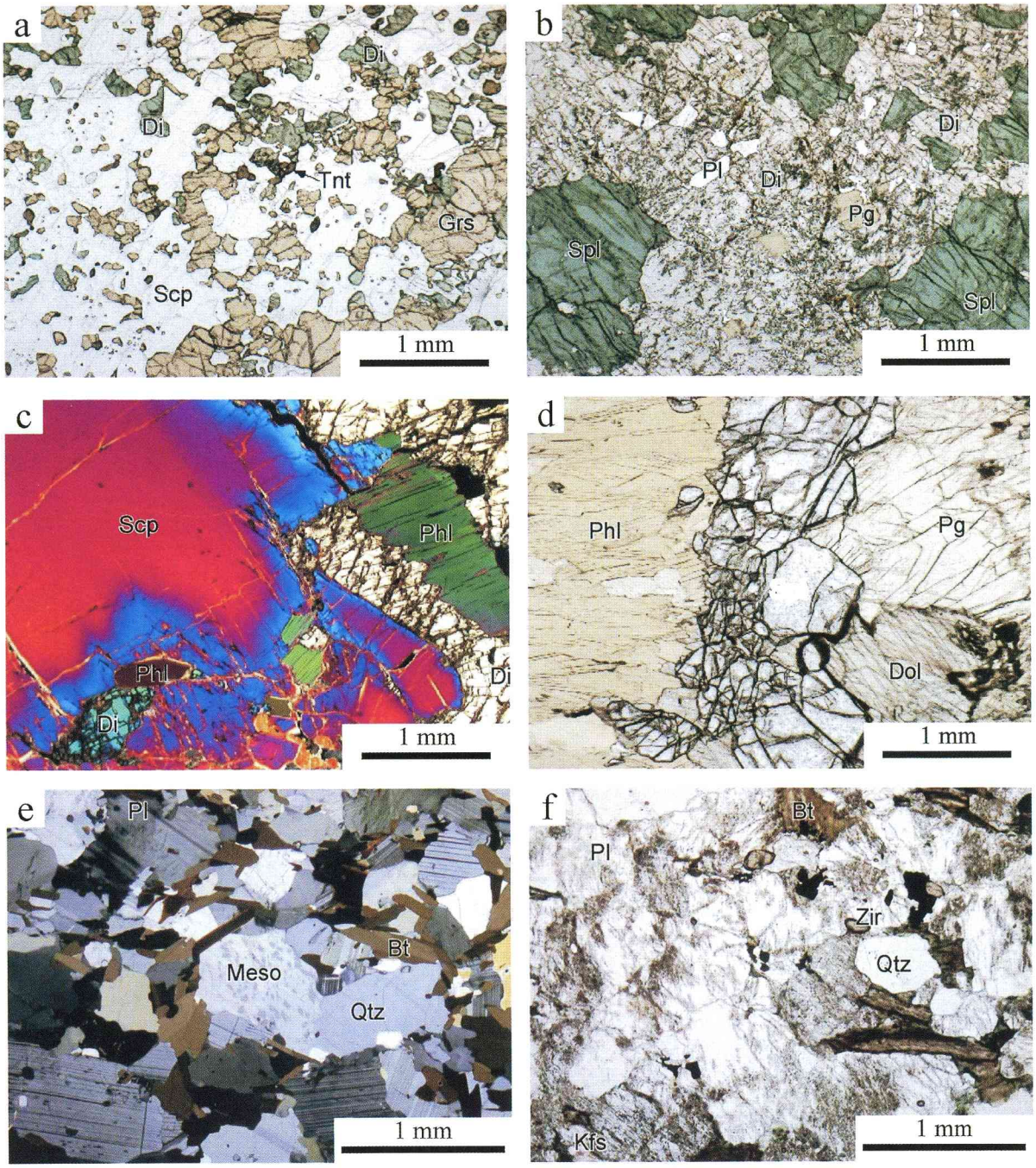

Plate 3-3. Photomicrographs of calc-silicate rocks (a~d) and granitic rocks (e~f). (a) Calc-silicate rock containing grossular (Grs), diopside (Di), scapolite (Scp), plagioclase and titanite (Tnt) collected from northern area. Plane-polarized light. (b) Green spinel (Spl)-diopside calc-silicate rock from southern area. Minor pargasite (Pg), plagioclase (Pl) and scapolite are also present. Plane-polarized light. (c) Characteristic zoned scapolite-bearing diopside-phlogopite (Phl) calc-silicate rock from southern area. Cross-polarized light. (d) Dolomite (Dol)-bearing spinel-phlogopite-pargasite calc-silicate rock from southern area. Colorless spinel has high-Mg content. Plane-polarized light. (e) Granitic gneiss consisting of biotite (Bt), plagioclase, quartz and methoperthite (Meso), showing a weak foliation. Cross-polarized light. (f) Muscovite-biotite granite dike consisting of plagioclase, biotite, K-feldspar (Kfs), quartz and muscovite with apatite and zircon (Zir). Plane-polarized light.

Antarctic Geological Map Series

Sheet 1	East Ongul Island 1:5,000	March 1974
Sheet 2	West Ongul Island 1:5,000	March 1974
Sheet 3	Teöya 1:5,000	March 1975
Sheet 4	Ongulkalven Island 1:5,000	March 1975
Sheet 5	Langhovde 1:25,000	March 1976
Sheet 6 & 7	Skarvsnes 1:25,000	March 1977
Sheet 8	Kjuka and Telen 1:25,000	March 1979
Sheet 9	Skallen 1:25,000	March 1976
Sheet 10	Padda Island 1:25,000	March 1977
Sheet 11	Cape Hinode 1:25,000	March 1978
Sheet 12	Lützow-Holm Bay 1:250,000	March 1989
Sheet 13	Prince Olav Coast 1:250,000	March 1989
Sheet 14	Sinnan Rocks 1:25,000	March 1983
Sheet 15	Cape Ryûgû 1:25,000	March 1980
Sheet 16	Akebono Rock 1:25,000	March 1986
Sheet 17	Niban Rock 1:25,000	March 1983
Sheet 18	Kasumi Rock 1:25,000	March 1984
Sheet 19	Tenmondai Rock 1:25,000	March 1985
Sheet 20	Akarui Point and Naga-iwa Rock 1:25,000	March 1984
Sheet 21	Cape Omega 1:25,000	March 1979
Sheet 22	Oku-iwa Rock 1:25,000	March 1981
Sheet 23	Honnör Oku-iwa Rock 1:25,000	March 1987
Sheet 24	Rundvågskollane and Rundvågshetta 1:25,000	March 1986
Sheet 25	Botnneset 1:25,000	March 1987
Sheet 26	Strandnibba 1:25,000	March 1985
Sheet 27 (1)	Mt. Fukushima, Northern Yamato Mountains 1:25,000	March 1978
Sheet 27 (2)	Mt. Torimai, Northern Yamato Mountains 1:25,000	March 1995
Sheet 28	Central Yamato Mountains, Massif B and Massif C 1:25,000	March 1982
Sheet 29	Belgica Mountains 1:25,000	March 1981
Sheet 30	Southern Yamato Mountains (Massif A and JARE-IV) 1:25,000	March 1988
Sheet 31	Balchenfjella 1:100,000	March 1991
Sheet 32	Widerøefjellet 1:100,000	March 1992
Sheet 33	Bergersenfjella 1:100,000	March 1993
Sheet 34	Brattnipene 1:100,000	March 1996
Sheet 35	Sør Rondane Mountains 1:250,000	March 1997
Sheet 36	Ongul Islands 1:10,000	March 1994
Sheet 37	Mount Riiser-Larsen 1:12,500	March 2000
Sheet 38	Tonagh Island 1:10,000	March 2001
Sheet 39	Skallen (Revised Edition) 1:10,000	March 2004